Appendix A: Publications and conference proceedings

Publications:

- Moyo L., Focke, W. W., Labuschagne, F. J., Heidenrich, D. & Radusch, H.-J. (2013) Properties of layered double hydroxide micro- and nanocomposites. *Materials Research Bulletin*. (48) 1218-1227.
- Moyo L., Focke, W. W., Labuschagne, F. J. & Verryn, S. (2012). Layered double hydroxide intercalated with sodium dodecyl sulphate *Mol. Cryst. Liq. Cryst.*, 555(1): 51–64.
- Focke, W.W., Nhlapo, N. S., Moyo, L. & Verryn, S. M. C. (2010). Thermal properties of lauric- and stearic acid-intercalated layered double hydroxides. *Mol. Cryst. Liq. Cryst.*, 521(1), 168–178.

Pending publications:

- Focke, W. W., Moyo L., Labuschagne, F. J. W. & Ramjee, S. Fatty acid intercalated hydrotalcite as a rheology modifier in Jojoba oil (November 2012).

Conference contributions:

- Moyo L, Heidenrich, D., Labuschagne, F. J., Radusch, H.-J. & Focke, W. W. (2011). Impact strength of LDH-St polymer composites. Poster presentation at the 15th International Conference on Polymeric Materials, Halle (Saale), Germany, September 2011.
- Moyo, L., Focke, W. W., Labuschagne F. J. & and Verryn, S. (2011). Layered double hydroxide intercalated with sodium dodecyl sulphate. Oral and poster presentation at the 11th International Conference on Frontiers of Polymers and Advanced Materials, Pretoria, South Africa, May 2011.
- Moyo, L, Heidenrich, D., Labuschagne, F. J., Androsch, R. & Focke, W. W. (2010). The effect of matrix polarity on the impact properties of LDH-stearate polymer composites. Poster presentation at the 14th International Conference on Polymeric Materials, Halle (Saale), Germany, September 2010.

Appendix B: Fatty acid-intercalated layered double hydroxides

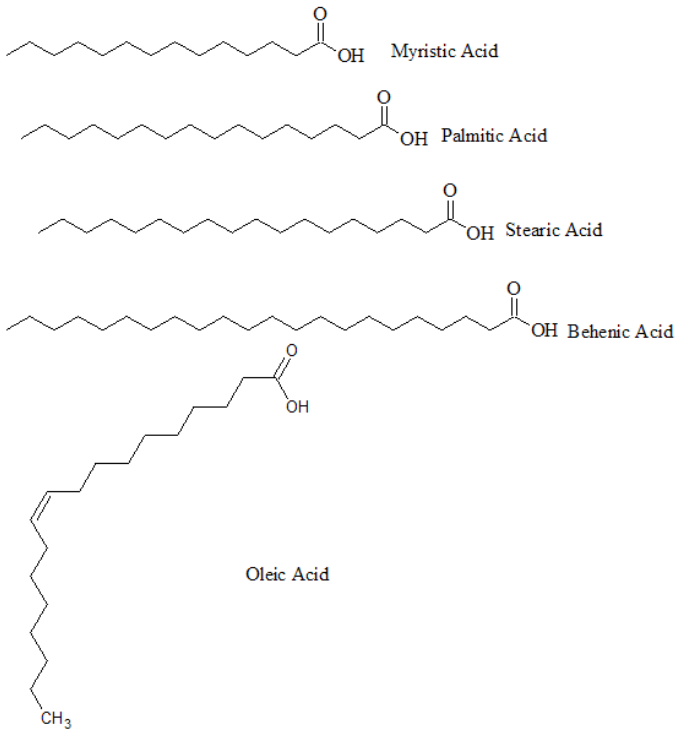

Figure B-1. Fatty/carboxylic acids used in the study

Figure B-1 shows the fatty acids used in the intercalation reaction. Oleic acid was also intercalated to demonstrate the close packing phenomenon. Due to the presence of the *cis*-double bond, the molecules pack with difficulty as this bond limits chain flexibility and decreases adhesion to adjacent chains. The limiting area of oleic acid is about 32 $Å^2$, which is much greater than that of saturated fatty acid chains, which is ≈ 21 $Å^2$.

The basic method was adapted from Nhlapo et al. (2008) for the one-pot synthesis. The LDH-carbonate precursor was obtained from Chamotte Holdings and used as is.

Table B-1. Summary of intercalation experiments

Sample I.D	AEC (Acid)	Temperature (°C)	pH
LDH- stearate A	4	80	~9-10
LDH- stearate B	4	80	~9-10
LDH- stearate C	4.5	80	~9-10
LDH-laurate/jojoba oil	2 lauric + 1 jojoba oil	85	~9-10
LDH-stearate/jojoba oil (1AEC)	1 stearic + 2 jojoba oil	85	~9-10
LDH-stearate/jojoba oil (2AEC)	2 stearic + 1 jojoba oil	85	~9-10
LDH-stearate/Jojoba oil (2AEC)	2 stearic + 1 jojoba oil	85	~9-10
LDHSt 1 AEC	1	80	~9-10
LDHSt 2AEC	2	80	~9-10
LDH-myristate 1	4	70	~9-10
LDH-myristate 2	4	70	~9-10
LDH-myristate 3	3	70	~9-10
LDH-myristate 4	4	70	~9-10
LDH- palmitate 1	3	75	~9-10
LDH-palmitate 2	4.5	75	~9-10
LDH- palmitate 3	4.5	75	~9-10
LDH- palmitate 4	4	75	~9-10
LDH-palmitate/stearate	2 palmitic + 2 stearic	80	~9-10
LDH-behenate 1	4	90	~9-10
LDH-behenate 2	3.5	90	~9-10

X-Ray Diffraction

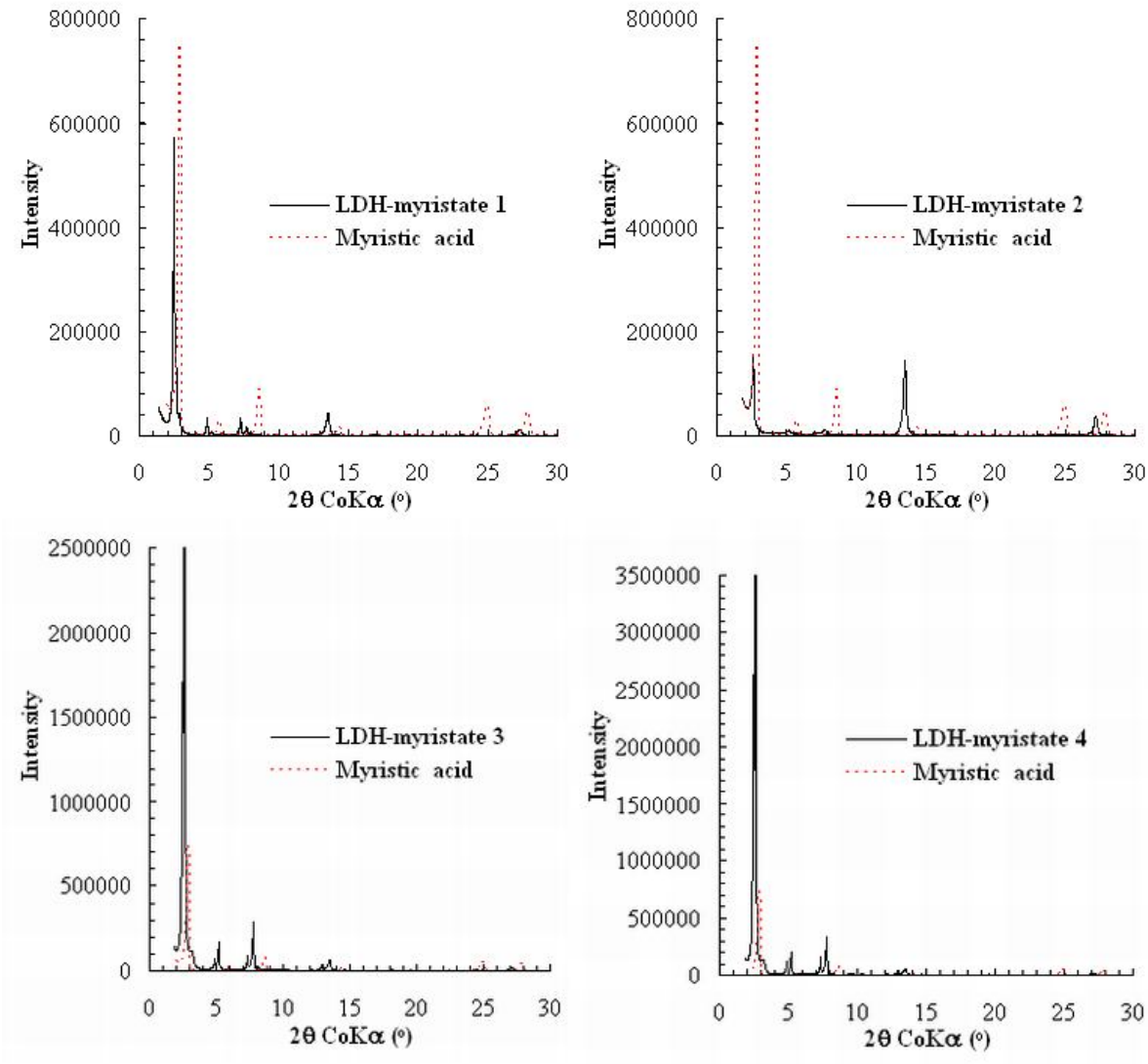

Figure B-2. XRD diffractograms for LDH-myristate

Table B-2. Observed 2θ reflections of XRD of neat myristic acid and LDH-myristate

Sample	Reflections					
	2θ(°)	d_{003}	2θ(°)	d_{006}	2θ(°)	d_{009}
Myristic acid	2.94	3.50	5.77	1.78	8.63	1.19
LDH-myristate 1	2.48	4.14	4.86	2.11	7.26	1.41
LDH-myristate 2	2.30	4.46	4.58	2.24	6.84	1.50
LDH-myristate 3	2.26	4.55	4.41	2.32	6.57	1.56
LDH-myristate 4	2.18	4.71	4.34	2.37	6.50	1.58

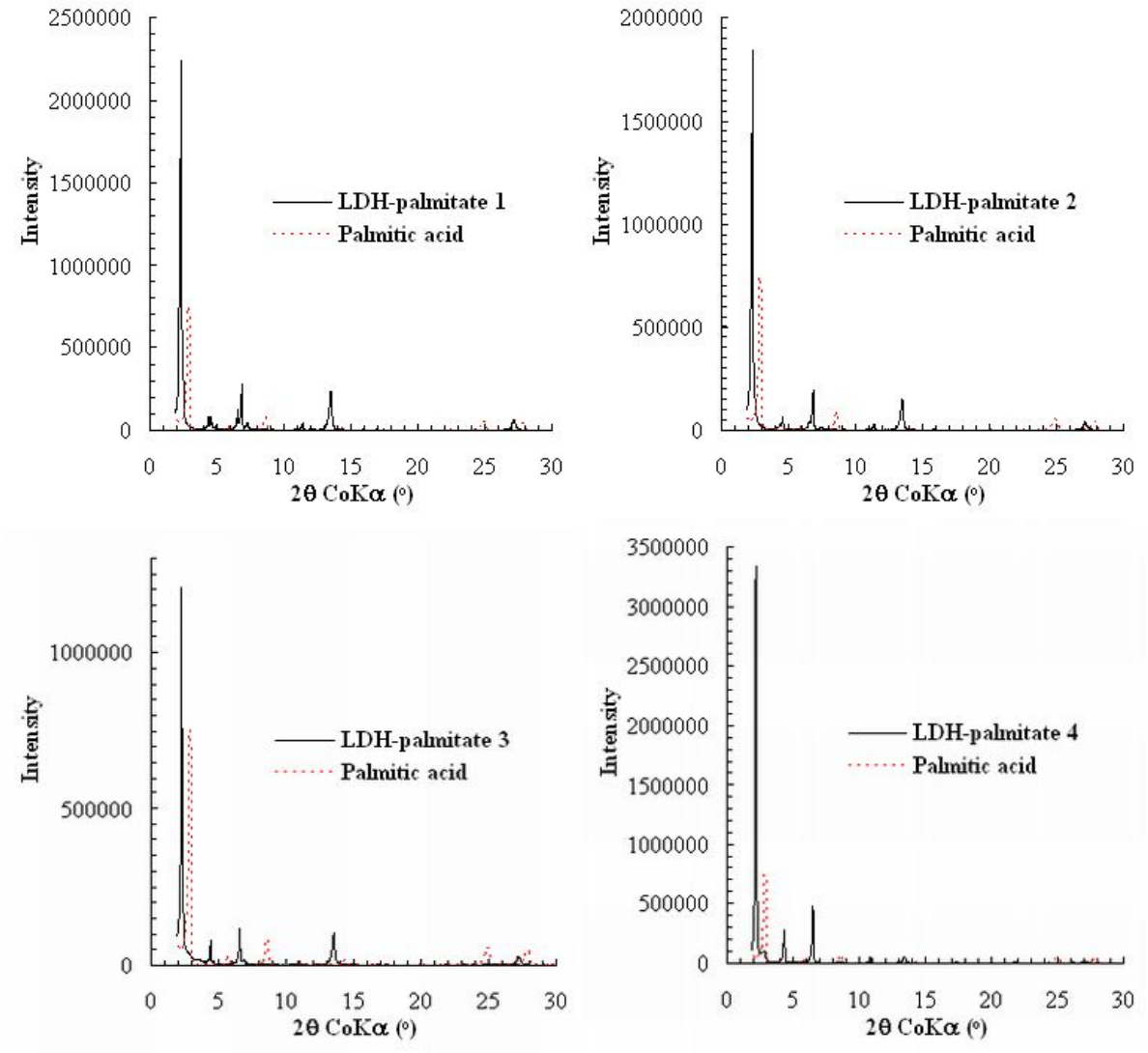

Figure B-3. XRD diffractograms for LDH-palmitate

Table B-3. Observed 2θ reflections of XRD of neat palmitic acid and LDH-palmitate

Sample	Reflections					
	2θ(°)	d_{003}(nm)	2θ(°)	d_{006}(nm)	2θ(°)	d_{009}(nm)
Palmitic acid	2.94	3.50	5.77	1.78	8.63	1.19
LDH-palmitate 1	2.32	4.43	4.60	2.23	6.86	1.50
LDH-palmitate 2	2.30	4.46	4.58	2.24	6.84	1.50
LDH-palmitate 3	2.26	4.55	4.41	2.32	6.57	1.56
LDH-palmitate 4	2.18	4.71	4.34	2.37	6.50	1.58

The average d-spacing observed for LDH-palmitate samples was 4.538 nm. However, it is clear that there are palmitic acid impurities in the case of LDH-palmitate 4. This further substantiates the observations by Kuehn and Poelmann (2010) that a second layer of undissociated acid will lead in greater d-spacings.

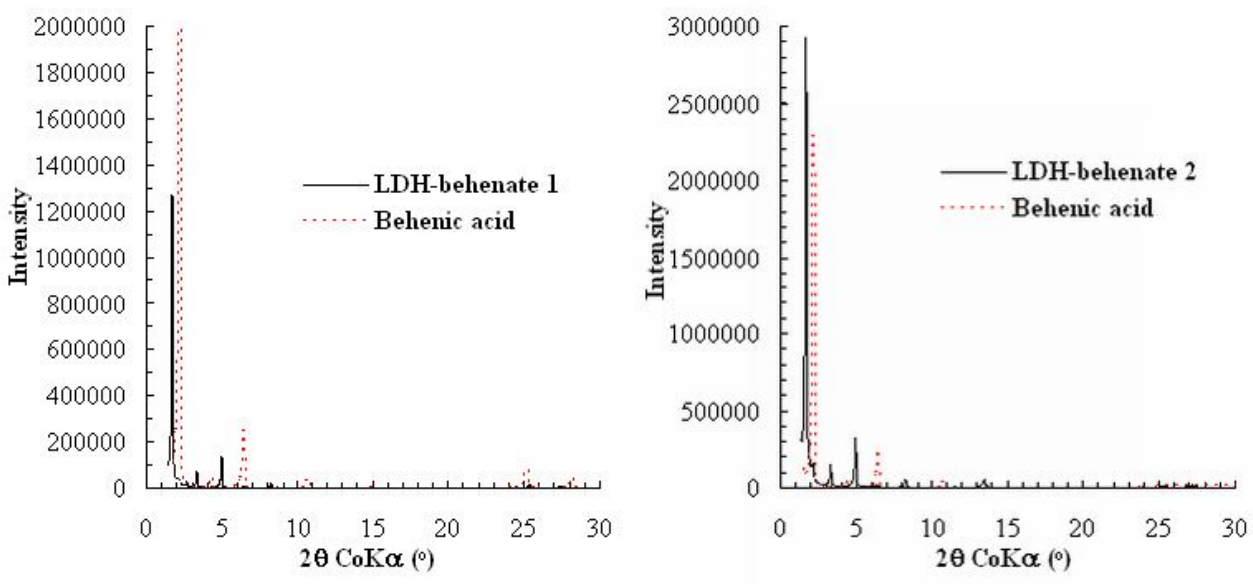

Figure B-4. XRD diffractograms for LDH-behenate

Table B-4. Observed 2θ reflections of XRD of neat behenic acid and LDH-behenate

Sample	Reflections					
	2θ(°)	d_{003}(nm)	2θ(°)	d_{006}(nm)	2θ(°)	d_{009}(nm)
Behenic acid	2.22	4.62	4.35	2.36	6.45	1.59
LDH-behenate 1	1.69	6.08	3.33	3.09	4.96	2.07
LDH-behenate 2	1.68	6.12	3.31	3.10	4.96	2.07

The average d-spacing observed for LDH-behenate samples was 6.097 nm.

Co-intercalation Trials

Two different fatty acids were used in the intercalation reaction, i.e. palmitic acid and stearic acid. The resultant intercalation product had a d-spacing of 4.56 nm (Figure B-5). This is substantially higher than what is normally obtained for bilayer LDH-palmitate (4.46 nm), yet it is lower than that of bilayer LDH-St (4.88 nm). This is an indication that the fatty acids will orient themselves in such a manner that they can accommodate each other, despite the difference in chain length.

In other scenarios, an attempt was made to co-intercalate Jojoba oil and stearic acid into LDH in a ratio of 2:1 and 1:2 respectively. However, co-intercalation was only observed in the later ratio of Jojoba oil to stearic acid (Figure B-5).

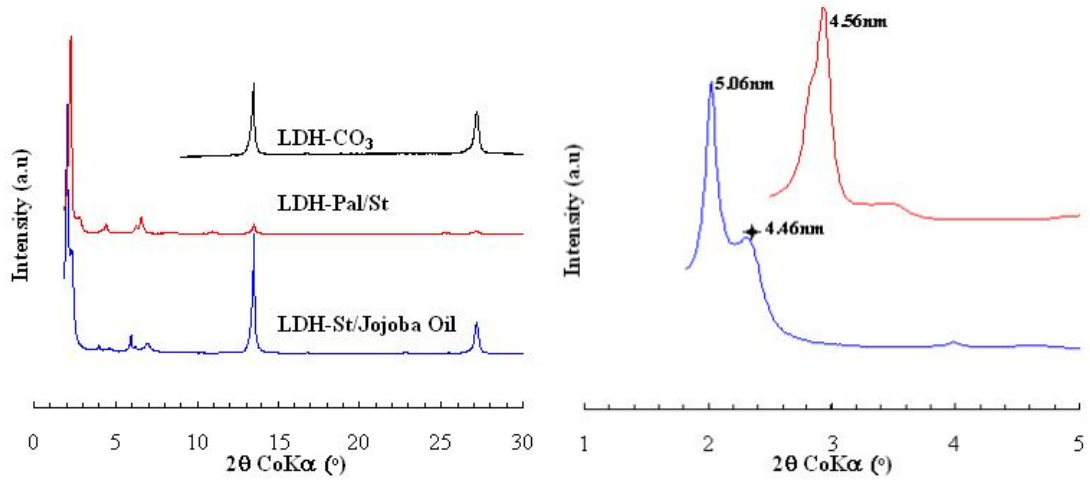

Figure B-5. XRD diffractogram of co-intercalated organo-LDH

Co-intercalation of stearate anion and Jojoba oil yielded a mixed-order product with crystallites with d-spacings of 5.06 and 4.46 nm. The latter is assumed to be a constituent of Jojoba oil; its phases are marked by means of asterisks in Figure B-5. This points to the possible exchange/incorporation of the Jojoba oil constituents with the LDH interlayer anions. The narrow symmetric peaks observed are indicative of a highly crystalline and well-ordered material. This is primarily explained by the fact that Jojoba oil wax esters have a chain length of C_{34}–C_{50} with an alcohol/acid combination of C_{16}–C_{26}, and hence allow interaction with the interlayer anions. The fatty acid and alcohol component of the ester is usually unsaturated, both possessing a cis-ethylenic bond between the 9th and the 10th carbon, counting from either of the terminal methyl groups (Miwa, 1984[3]). The cis-geometry has bends at the position of the double bond. The ill-defined secondary peak is due to co-intercalation of a Jojoba oil constituent. However, as mentioned earlier, the fact that the Jojoba oil esters possess a double bond imposes some steric challenges. Hence, minimal intercalation is observed as well as poor ordering/absorption within the interlayer.

Table B-5 shows the elemental composition as determined by ICP-EOS.

Table B-5. Compositional data and formulae of co-intercalated organo-LDHs

Intercalated Anion	**Aluminium mol ratio to**		
	Mg	**Na**	***x***
Carbonate	2.33	0.14	0.30
Pal/St	2.33	0.02	0.30
St/Jojoba oil	1.80	0.29	0.36

[3] Miwa, T.K. (1984). Structural determination and uses of Jojoba Oil. Journal of the American Oil Chemists'Society. 61(2), 407E410.

Morphology

Figure B-6 shows the typical platelet morphology of the co-intercalated LDHs described above.

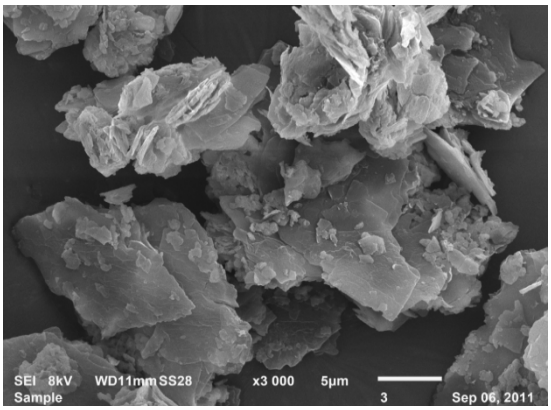

LDH- Stearate /Palmitate

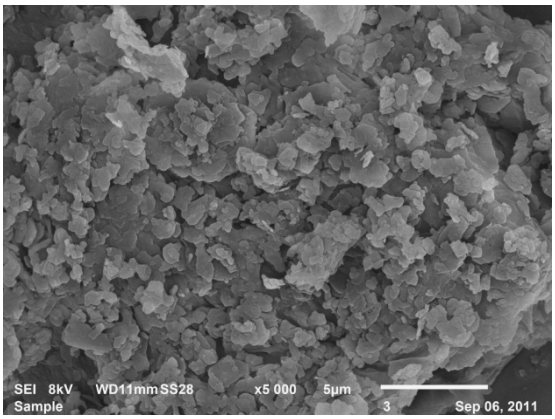

LDH- Jojoba oil/ Stearate

Figure B-6. SEM micrographs of co-intercalated LDHs

EDS Analysis of Clay Platelets

During the study some samples showed unusually high AEC levels or elavated levels of organic incorporation. For this reason the composition of the clay platelets was investigated.

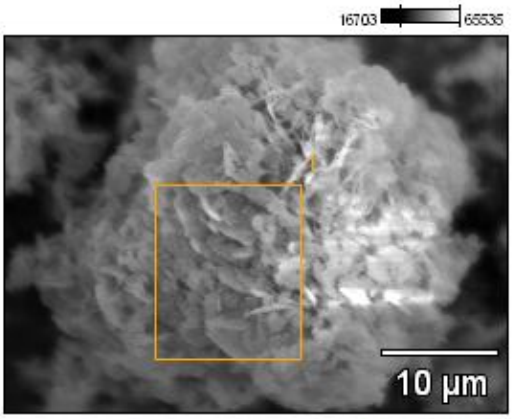

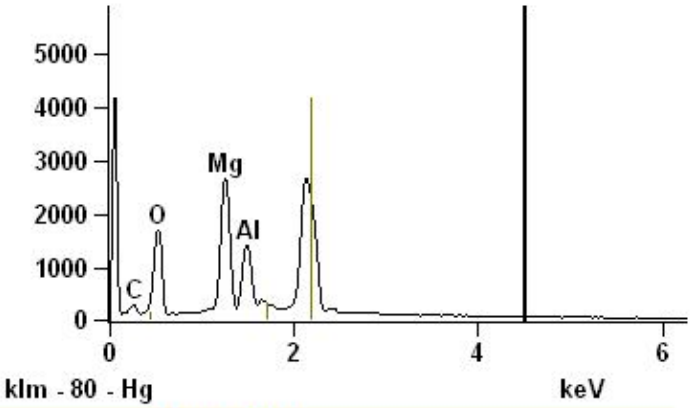

	Weight %		Atom ratio		
	Mg	Al	Mg	Al	Mg/Al Ratio
LDH-CO_3_pt1	28.6	16.6	1.06	0.64	1.72

Weight % Error (+/- 1 Sigma)

	O	*Mg*	*Al*
LDH-CO_3 pt1	+/-0.6	+/-0.3	+/-0.3

Figure B-7. LDH-CO_3 SEM micrograph, X-ray and composition of platelets

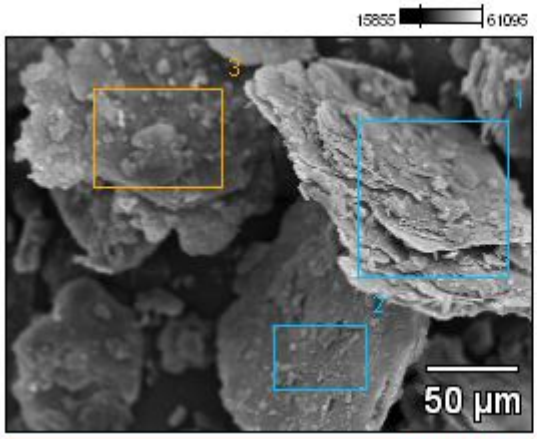

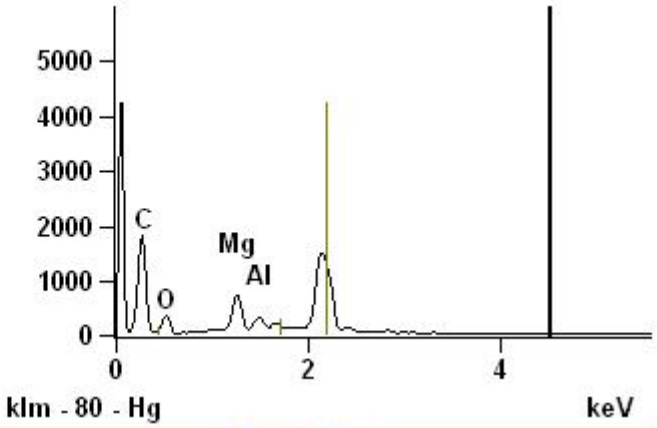

	Weight %		Atom ratio		
	Mg	Al	Mg	Al	Mg/Al ratio
LDH-myristate_pt1	31.2	13.6	1.03	0.50	2.58
LDH-myristate_pt2	27.1	10.3	1.12	0.39	2.88
LDH-myristate_pt3	28.6	14.5	1.19	0.54	2.22

Weight % Error (+/- 1 Sigma)

	Mg	Al
LDH-myristate_pt1	+/-0.7	+/-0.8
LDH-myristate_pt2	+/-0.4	+/-0.6
LDH-myristate_pt3	+/-0.6	+/-0.7

Figure B-8. LDH-myristate SEM micrograph, X-ray and composition of platelets

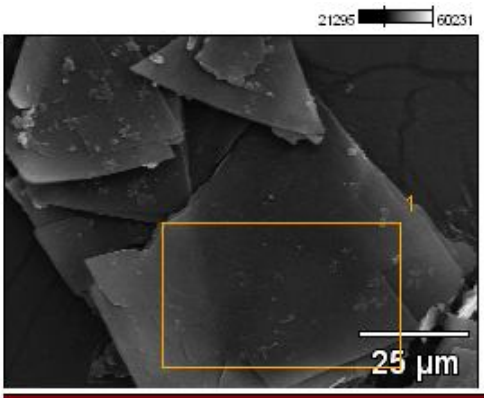

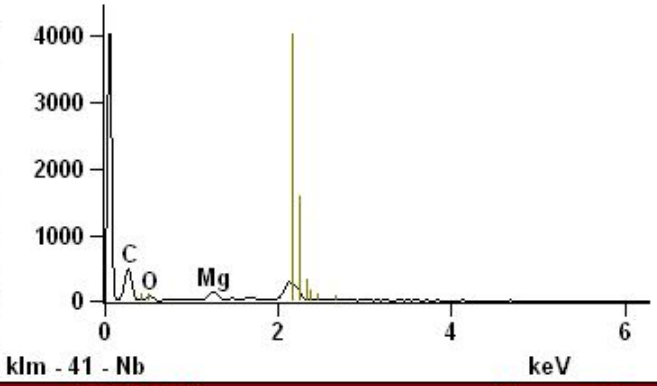

	Weight %	Atom ratio
	Mg	Mg
LDH-palmitate_pt1	44.7	1.86

Weight % Error (+/- 1 Sigma)

	Mg
LDH-palmitate_pt1	+/-2.3

Figure B-9. LDH-palmitate SEM micrograph, X-ray and composition of platelets

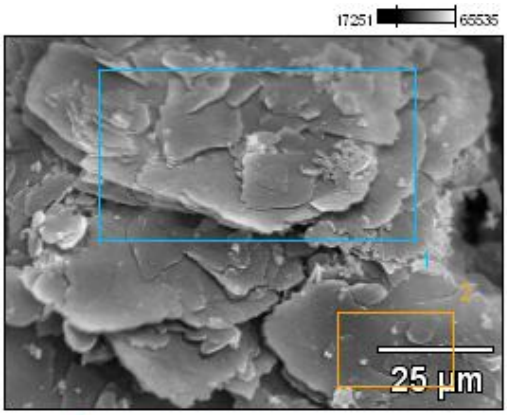

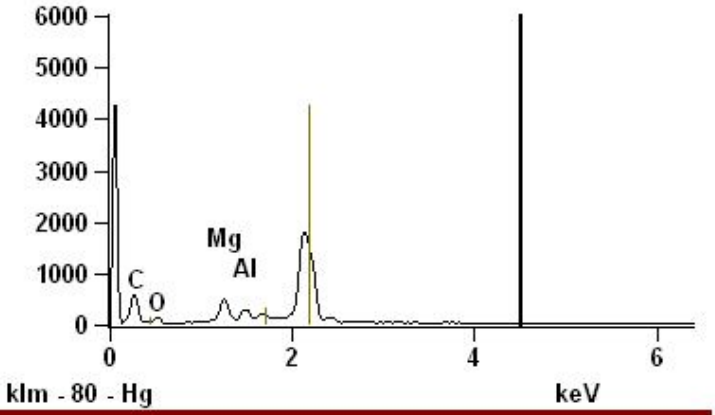

	Weight %		Atom ratio		
	Mg	Al	Mg	Al	Mg/Al ratio
LDH-stearate_pt1	21.3	12.6	0.89	0.47	1.90
LDH-stearate_pt2	34.9	19.3	1.45	0.71	2.03

Weight % Error (+/- 1 Sigma)

	Mg	Al
LDH-stearate_pt1	+/-0.5	+/-0.7
LDH-stearate_pt2	+/-1.0	+/-1.5

Figure B-10. LDH-St SEM micrograph, X-ray and composition of platelets

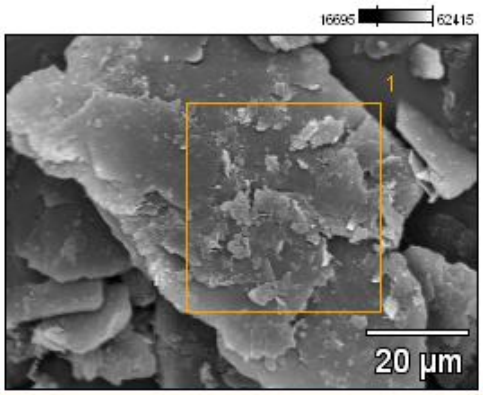

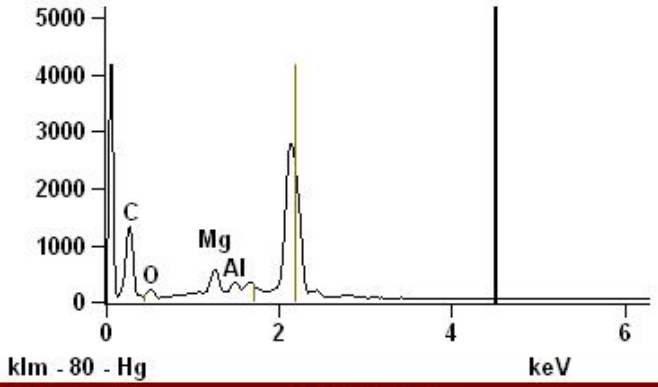

	Weight %		Atom ratio		
	Mg	Al	Mg	Al	Mg/Al ratio
LDH-behenate_pt1	17.8	10.8	0.74	0.4	1.85

Weight % Error (+/- 1 Sigma)

	Mg	Al
LDH-behenate_pt1	+/-0.6	+/-0.9

Figure B-11. LDH-behenate SEM micrograph, X-ray and composition of platelets

Thermogravimetric Analysis

The formulae used in the calculation of the clay content on a dry basis; actual clay and percentage organic content are:

$$\text{Clay content on a dry basis} = \frac{\%\ \text{Residue at 900 °C}}{\%\ \text{Residue at 150 °C}}$$

Actual clay content is obtained by multiplying the ratio of the clay content on a dry basis to that of 100% clay of the LDH precursor. For example, using LDH-CO_3,

Clay content on a dry basis = 57.33/98.51
= 58.19%

Ratio of clay on a dry basis to 100% = 100/58.19
= 1.718

% Organic content = 100 – Actual % clay

Table B-6. Summary of thermogravimetric data and estimates for the degree of intercalation

Sample identity	Residual mass loss (wt.%) at		Carboxylate/Al mol ratio
	150 °C	900 °C	
LDH-CO_3	98.10	57.68	-
LDH-myristate 1	92.90	23.63	1.19
LDH-myristate 2	96.88	14.61	2.64
LDH-myristate 3	97.77	48.59	0.17
LDH-myristate 4	96.83	13.65	2.88
LDH-palmitate 1	95.99	21.05	1.36
LDH-palmitate 2	96.23	20.54	1.42
LDH-palmitate 3	95.50	26.54	0.90
LDH-palmitate 4	95.73	14.92	2.24
LDH-stearate	95.40	13.11	2.39
LDH-behenate 1	96.45	8.71	3.36
LDH-behenate 2	96.04	10.72	2.60

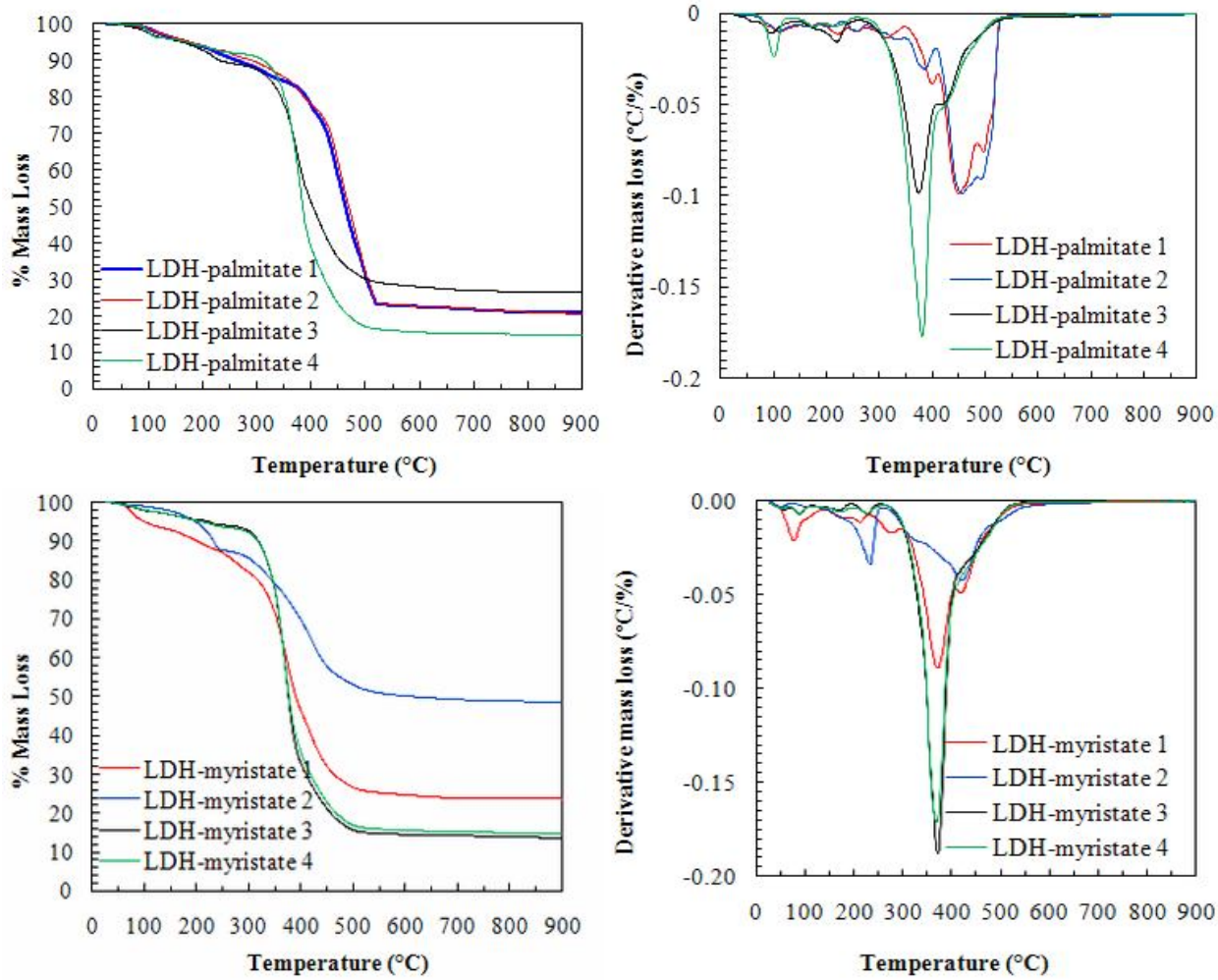

Figure B-12. LDH-palmitate and myristate TG profile

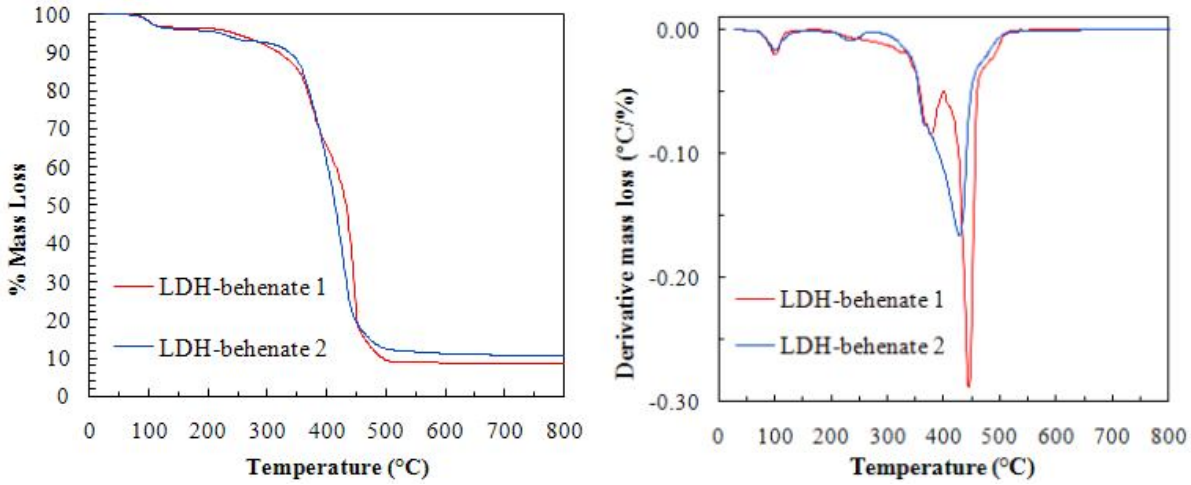

Figure B-13. LDH-behenate TG profile

Table B-7. Summary of thermogravimetric data, estimates for the degree of intercalation and d-spacing

Sample identity	Residual mass loss (wt.%) at		Carboxylate/Al mol ratio	d-spacing (nm)
	150 °C	900 °C		
LDH-CO_3	98.10	57.68	-	0.76
LDH- stearate 1	95.15	15.05	1.98	5.06
LDH- stearate 2	95.10	13.30	2.34	4.93
LDH- stearate 3	94.29	13.66	2.23	4.94
LDH- stearate 4	94.75	11.80	2.72	5.04
LDH- stearate 5	95.40	13.11	2.39	4.98
LDH- stearate 6	95.28	13.55	2.29	4.95
LDH- stearate 7	95.18	14.92	2.01	4.93
LDH- stearate 8	95.44	13.78	2.24	4.89
LDH- stearate 9	95.57	11.62	2.80	4.95
LDH- stearate 10	94.71	11.17	2.91	5.00
LDH- stearate 11	94.94	11.29	2.88	5.06
LDH- stearate 12	94.99	10.84	3.03	5.02
LDH- stearate 13	94.68	10.29	3.22	4.68
Average	95.04	12.64	2.54	4.96
Standard deviation	0.36	1.56	0.40	0.10
LDH- stearate 14	95.27	9.29	3.67	4.98
LDH- stearate 15	95.27	9.62	3.52	4.94
LDH- stearate 16	95.52	9.73	3.48	4.98
Average	95.35	9.55	3.56	4.97
Standard deviation	0.14	0.23	0.10	0.02

The division indicates samples prepared by two different individuals. The bottom three exhibit exceptionally high carboxylate/Al mol ratios. Discrepancies could have arisen from the pH regulation during synthesis, as well as the washing procedure used for the sample.

Appendix C: LDH-based polymer composites

Injection Moulding Comments

Table C-1. Injection moulding comments on EVA and derivative composites

Mould:	ASTM T.S		
		Set point	**Indicated**
Temperatures:		(°C)	(°C)
	Barrel 1	170	170
	Barrel 2	175	176
	Barrel 3	180	182
	Melt	180	182
	Mould	-	RT
Injection time		12 s	
Injection speed		8 mm/s	
Injection pressure		180 bar	
Hold on pressure		85 bar	
Back pressure		10 bar	
Screw speed		50 %	
Cooling time		25 s	
Stroke		22 mm(g)	
Clamping force		350 kN	
Remarks:		Fed with difficulty Moulded with ease Mouldings very rubbery Moulded all samples under the same moulding conditions Short cycle times	

Table C-2: Injection moulding comments on EVAL and derivative composites

Mould:	ASTM T.S		
		Set point	**Indicated**
Temperatures:		(°C)	(°C)
	Barrel 1	190	189
	Barrel 2	195	195
	Barrel 3	200	200
	Melt	200	200
	Mould	-	RT
Injection time		15 s	
Injection speed		15 mm/s	
Injection pressure		180 bar	
Hold on pressure		85 bar	
Back pressure		10 bar	
Screw speed		50 %	
Cooling time		25 s	
Stroke		22 mm(g)	
Clamping force		350 kN	
Remarks:		Fed with ease	
		Moulded with ease but stuck to the stationary half of the mould	
		Mouldings very hard	
		Moulded all samples under the same moulding conditions	
		Mouldings hammered out after each shot; long cycle time	

Table C-3. Injection moulding comments on LLDPE and derivative composites

Mould:	ASTM T.S		
		Set point	**Indicated**
Temperatures:		(°C)	(°C)
	Barrel 1	220	219
	Barrel 2	210	210
	Barrel 3	200	200
	Melt	191	190
	Mould	-	RT
Injection time		10 s	
Injection speed		10 mm/s	
Injection pressure		180 bar	
Hold on pressure		75 bar	
Back pressure		10 bar	
Screw speed		50 %	
Cooling Time		25 s	
Stroke		22 mm(g)	
Clamping force		350 kN	
Remarks:		Fed with ease	
		Moulded with ease	
		Mouldings tended to shrink	
		Moulded all samples under the same moulding conditions	

Polymer resin product sheets

Polymer-E 百利滿-E

Ethylene-Vinyl Acetate Copolymer Resin

乙烯醋酸乙烯酯樹脂

產品 Products / 物性 Physical Properties		單 位 Unit	檢驗方法 Test Method (ASTM)	發泡及鑄膜級 Foaming & Casting Grades		
				EV101	EV102	EV103
主要用途 Application				鞋材 運動器材 發泡 流延膜 Shoe Soles Sport Goods Foaming Extrusion Casting	鞋材 運動器材 發泡 流延膜 Shoe Soles Sport Goods Foaming Extrusion Casting	鞋材 運動器材 發泡 流延膜 Shoe Soles Sport Goods Foaming Extrusion Casting
特 性 Characteristics				優異的發泡加工性 優異的成品物性 Good Processability Good Physical Properties	優異的發泡加工性 優異的成品物性 Good Processability Good Physical Properties	優異的發泡加工性 優異的成品物性 Good Processability Good Physical Properties
熔融指數 / Melt Index		公克/10分鐘 g/10min	D1238	1.8	1.5	1.5
密度 / Density		公克/立方公分 g/cm³	D1505	0.941	0.938	0.943
混濁度 / Haze		%	D1003	-	-	-
光澤度 (60°) / Gloss (60°)		%	D523	-	-	-
抗衝擊強度 / Impact Strength		公克，50% F g/50% Failure	D1709	-	-	-
摩擦係數 / Coefficient of Friction		—	D1894	-	-	-
斷裂點抗張強度 Ultimate Tensile Strength (薄膜) (Film)	MD	公斤/平方公分 Kg/cm²	D882	-	-	-
	TD			-	-	-
(模壓)/ (Molded)			D638	210	200	220
1%伸長彈性係數 1% Secant Modulus (薄膜) (Film)	MD	公斤/平方公分 Kg/cm²	D882	-	-	-
	TD			-	-	-
伸長率 Elongation (薄膜) (Film)	MD	%	D882	-	-	-
	TD			-	-	-
(模壓)/ (Molded)			D638	730	700	750
抗撕裂強度 Tear Strength (薄膜) (Film)	MD	公斤/公分 Kg/cm	D1922	-	-	-
	TD			-	-	-
低溫脆裂溫度 Low Temperature Brittleness		℃	D746	<-70	<-70	<-70
韋氏軟化點 Vicat Softening Point		℃	D1525	65	73	63
硬度 Hardness		蕭氏 D Shore D	D2240	35	38	33
熱變形溫度 (66 psi) Heat Deflection Temp. (66 psi)		℃	D648	40	42	38
熔點 / Melting Point		℃	APC Method	82	86	79
醋酸乙烯含量 / VA Content		%	APC Method	18	14	21

Notes： (1) For general purpose and thin gauge film applications, film properties are based on thickness of 1.25 mil (32 micron) extruded on a blown film line at 330°F(165℃) and 2.1 BUR. For Heavy Duty films, properties are based on thickness of 7mil(180micron) and blown at 420°F (215℃) and blow-up ratio 1.8:1.

(2) The data reported are typical properties for reference only and are not to be construed as specification.

說明： (1) 上述之抗張強度、光學性、抗衝擊強度等各項物性是以 50 m/m，L/D 26:1 之擠壓機，吹袋比 2.1:1 和1.8:1 條件，製出厚度為 32 micron/180 micron薄膜樣品之測試結果。

(2) 上述資料均經本公司細心編撰，惟因使用情況之變化，非受本公司控制，恕不負保證之責。

LLDPE - Product Data Sheet

HR 411 LLDPE

Date of Issue: February 2002 **Print Date: July 2002**

Information
Polymer technology centre
P O Box 72
Modderfontein 1645
South Africa

Tel: +27 (0) 11 458 0700
Fax: +27 (0) 11 458 0734

Polyethylene sales
Sasol Polymers
Johannesburg
Tel: +27 (0) 11 790 1250
Cape Town
Tel: +27 (0) 21 686 7740
Durban
Tel: +27 (0) 31 267 0777

www.sasol.com/polymers

sasol
reaching new frontiers

Sasol Polymers
Polythene Business

Rotational moulding/injection moulding

Melt index: 3.5 Density: 0.939

Features	Additives	Applications
High rigidity	Antioxidant	Large mouldings
Excellent impact strength		Thick walled containers
Excellent chemical resistance		Articles for indoor use
Good ESCR		
Tough and abrasion resistant		
Colourable		
Hexene copolymer		

Performance properties - HR 411

Test	Value	Unit	Test method
MFI (190°C/2.16kg)	3.5	g/10min	ASTM D1238
Nominal density	0.939	g/cm^3	ASTM D1505
Tensile strength at yield	19	MPa	ASTM D638 [1)]
Tensile strength at break	24	MPa	ASTM D638 [1)]
Elongation at break	820	%	ASTM D638 [1)]
Flexural modulus	846	MPa	ASTM D790
ESCR F_{50}	>500	hr	ASTM D1693 [2)]
Impact energy at -40°C	35	J/mm	ASTM D3029 [3)]
Vicat softening temperature	121	°C	ASTM D1525
Shore D hardness	61	Shore D	ASTM D2240

[1)] Crosshead speed 50mm/min
[2)] 100% Igepal C0630
[3)] Tested on rotomoulded product

ARMSA MEMBER

LLDPE - Product Data Sheet

sasol
reaching new frontiers

Processing (Rotomoulding)

An air temperature of 270˚C to 300˚C is recommended for processing of HR 411. Temperatures above 300˚C should be avoided as this would narrow the processing window considerably and could result in poor physical properties.

Processing (Injection moulding)

HR 411 has a medium melt viscosity making it unsuitable for moulds with long flow paths. Typical melt temperatures would be 200˚C - 280˚C. Parts can be demoulded at relatively high temperatures due to the material's high melting point and rigidity.

Typical temperature profile (Injection moulding)

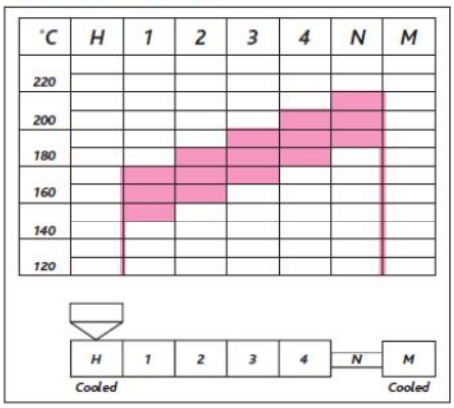

Presentation

Supplied in pellet form packed in 25kg bags. Grinding of pellets is required to make it suitable for rotomoulding.

Handling

Workers should be protected from the possibility of skin or eye contact with molten polymer. Safety glasses are suggested as a minimal precaution to prevent possible mechanical or thermal injury to the eyes. Fabrication areas should be ventilated to carry away fumes or vapours.

Combustibility

Polyethylene resins will burn when supplied with adequate heat and oxygen. They should be handled and stored away from contact with direct flames and/or other ignition sources. In burning, polyethylene resins contribute high heat and may generate a dense black smoke. Fires can be extinguished by conventional means, with water and water mist preferred. In enclosed areas, fire fighters should be provided with self-contained breathing apparatus.

Pigmentation (Rotomoulding)

For colouring purposes inorganic pigments should be added at the lowest possible concentration and mixed in using a high speed mixer or a tumble blender, prior to moulding. Pigment preparations should contain only minimal amounts of dispersants.

Food Packaging

This material complies with F&DA regulation 177.1520 when used unmodified and according to good manufacturing practices for food contact applications. Accordingly, this material may be used in all food contact applications (except holding food during cooking).

Conveying

Conveying equipment should be designed to prevent accumulation of fines and dust particles that are contained in all polyethylene resins. These fines and dust particles can, under certain conditions, pose an explosion hazard. We recommend the conveying system used:

1. be equipped with adequate filters;
2. is operated and maintained in such a manner to ensure no leaks develop;
3. that adequate grounding exists at all times.

We further recommend good housekeeping be practised throughout the facility.

Storage

As ultraviolet light may cause a change in the material, all resins should be protected from direct sunlight during storage.

EVAL EUROPE
Building better barriers

Datasheet **Typical Properties of EVAL™ Resin**

EVAL™ T101B

	Test method		Unit	Value
Ethylene Content	Kuraray Method		mol %	32
Oxygen Transmission Rate	ISO 14663-2 annexC	20°C 0%RH	cm³.20µm/m².day.atm	0.23
	ISO 14663-2 annexC	20°C 35%RH	cm³.20µm/m².day.atm	
	ISO 14663-2 annexC	20°C 50%RH	cm³.20µm/m².day.atm	
	ISO 14663-2 annexC	20°C 65%RH	cm³.20µm/m².day.atm	0.5
	ISO 14663-2 annexC	20°C 85%RH	cm³.20µm/m².day.atm	1.8
	ISO 14663-2 annexC	20°C 90%RH	cm³.20µm/m².day.atm	
	ISO 14663-2 annexC	20°C 100%RH	cm³.20µm/m².day.atm	
Water Vapour Transmission Rate	ASTM E96-E		g.30µm/m².day.	37
Density	ISO 1183		kg/m³	1.17
Yield Stress	ISO 527		MPa	
Stress at Break	ISO 527		MPa	
Yield Strain	ISO 527		%	
Strain at Break	ISO 527		%	
Young's Modulus	ISO 527		MPa	
Flexural Modulus	ISO 178		MPa	
Izod Impact Strength	ISO 180		kJ/m²	
Izod at -40°C	ISO 180			
Charpy Impact Strenght	ISO 179-1		kJ/m²	
Charpy at -40°C	ISO 179-1		kJ/m²	
Rockwell Hardness	ISO 2039-2		M	
Melting Temperature	ISO 11357		°C	183
Crystalisation Temperature	ISO 11357		°C	161
Glass Transition Point	ISO 11357		°C	69
Vicat Softening Point	ISO 306		°C	
Melt Mass-Flow Rate	ISO1133	190°C	g/10min	1.7
	ISO1133	210°C	g/10min	4.3
	ISO1133	230°C	g/10min	
	ISO1133	250°C	g/10min	

Contact:	EVAL Europe nv Haven 1053 - Nieuwe Weg 1, bus 10 2070 Zwijndrecht (Antwerp), Belgium Tel +32 3 250 9733 Fax +32 3 250 9745
Data updated on:	18-nov-04
Layout updated on:	11-dec-06

Note - The information and data contained in this document are believed to be correct and are given in good faith. However, no liability, warranty or guarantee of final product performance is created by this document. No freedom from any patent is granted or to be inferred. This document does not constitute a sales specification and the EVAL Europe nv Sales Contract General Terms and Conditions continue to apply.

kuraray

EVAL Europe nv | Haven 1053 | Nieuwe Weg 1 - Bus 10 | B-2070 Zwijndrecht (Antwerp) | Belgium
Telephone +32 3 250 97 33 | Fax +32 3 250 97 04 | www.eval.be | VAT BE 0461.831.747 | RPR Antwerpen

FT-IR of Composites

Figure C-1 shows the FTIR results of the LDH-stearate and each of the 10 wt% composites prepared. The LDH-CO_3 exhibits a broad band at 3455 cm^{-1}, which is characteristic of the hydroxyl stretching vibration of free hydrogen, hydrogen bonded to the octahedral layer and water molecules. The LDH-CO_3 has a peak at 1360 cm^{-1}, which is attributed to carbonate anions. For the LDH-St there is minimal carbonate contamination as the peak within the specified area is weak or in some cases absent. The OH stretching vibrations are also observed, as well as a shoulder between 3247 and 3225 cm^{-1}, which is attributed to the water molecules bonded to the interlayer anion by hydrogen bonding. The peaks between 2940 and 2847 cm^{-1} are assigned to -CH_2 asymmetric and symmetric vibrations of aliphatic groups, while the peaks at 1630 and 1462 cm^{-1} are due to O-H deformation of entrapped water molecules and CH_2 deformation respectively. The CH_2 wagging modes are also observed in the 1300–1250 cm^{-1} range. The 1534 cm^{-1} peak is due to the symmetric stretching mode of the ionised –C-O group. The M-O in-plane stretching and deformation of the LDH metal lattice is observed between 1000 and 719 cm^{-1}. Generally, all these peaks are preserved in the composite materials. However, a few peaks from the polymer overlap with those in the LDH stearate, e.g. the OH band overlaps with that of the LDH-St and EVAL due to the existence of OH groups in the polymer itself. However, the –OH band in the EVAL/LDH-St composite broadens and its intensity is reduced. This could be attributed to the interaction of the –OH groups of the metal hydroxide with that of the polymer. This band is retained in the EVA and LLDPE composites, pointing to no interaction of the aforementioned functional groups. The peaks at 1735 and 1235 cm^{-1} in the EVA samples are a result of O-C=O carbonyl stretching vibrations of the ester and asymmetric vibration of the C-O-C bond respectively.

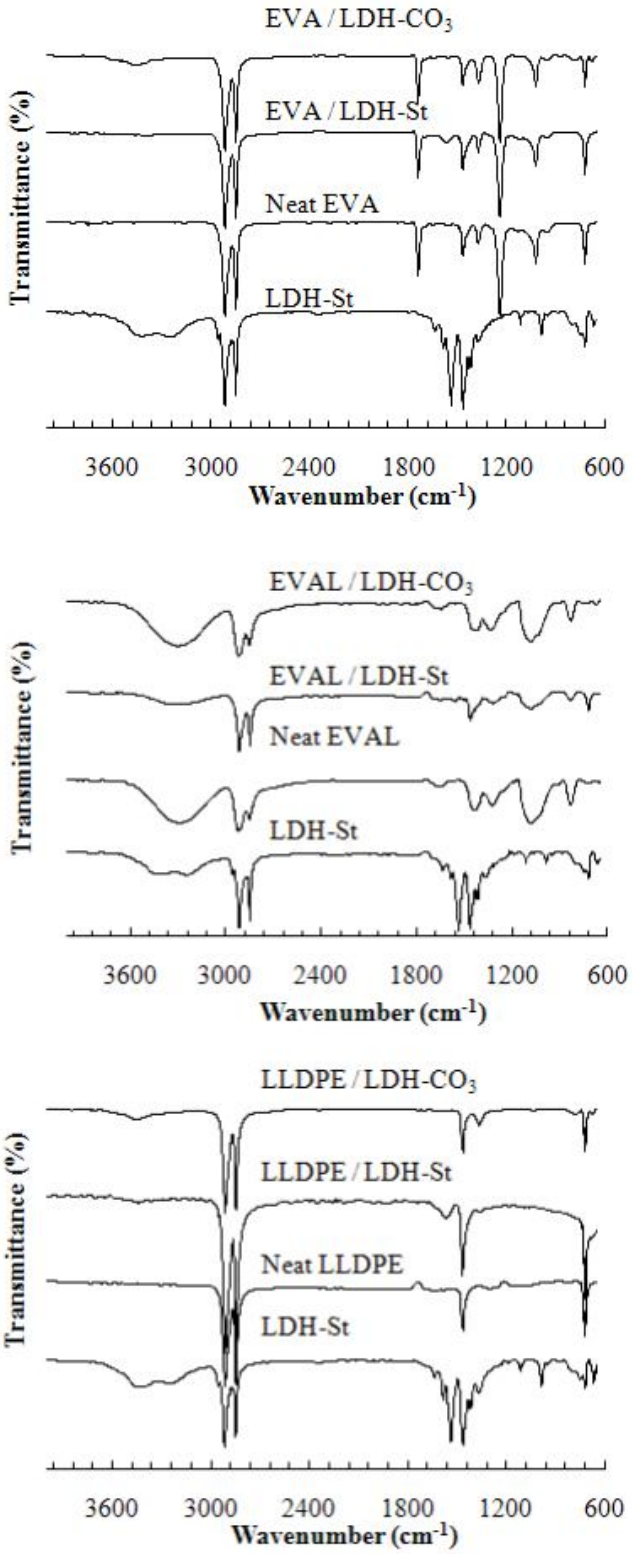

Figure C-1. FTIR of the neat and composite derivatives

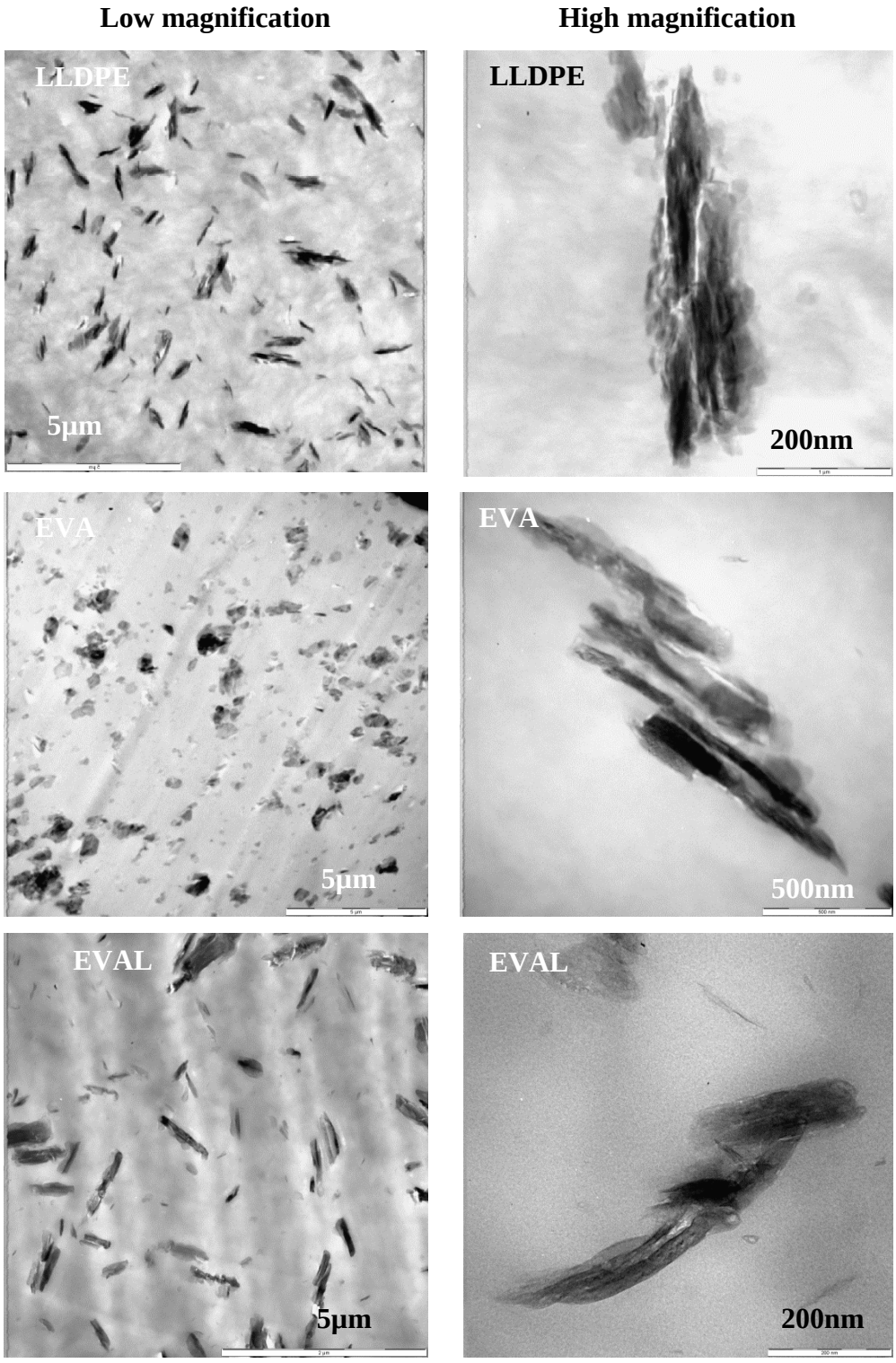

Figure C-2. TEM micrographs of the 5 wt.% LDH-carbonate polymer composites

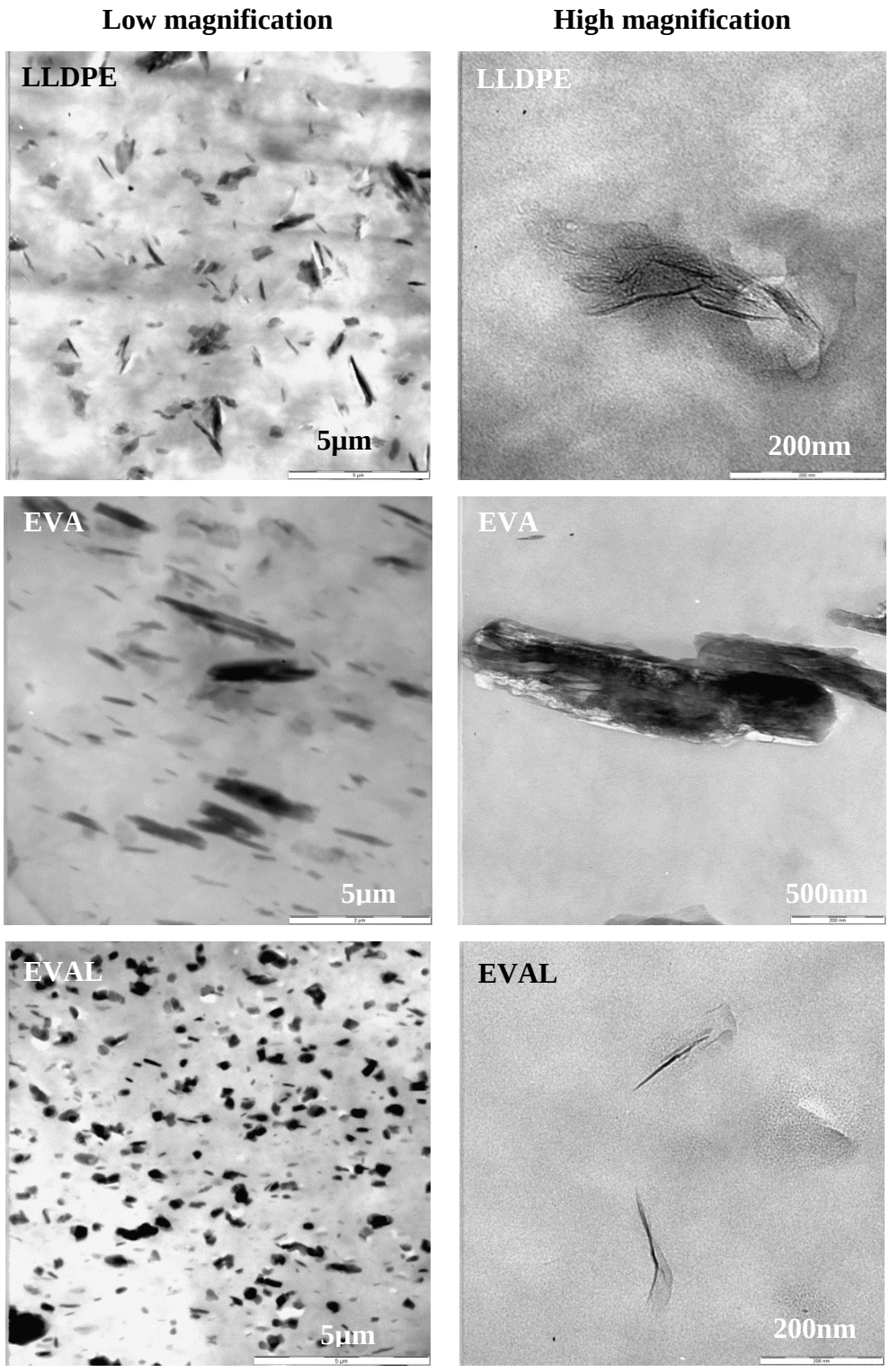

Figure C-3. TEM micrographs of the 5 wt.% LDH-stearate polymer composites

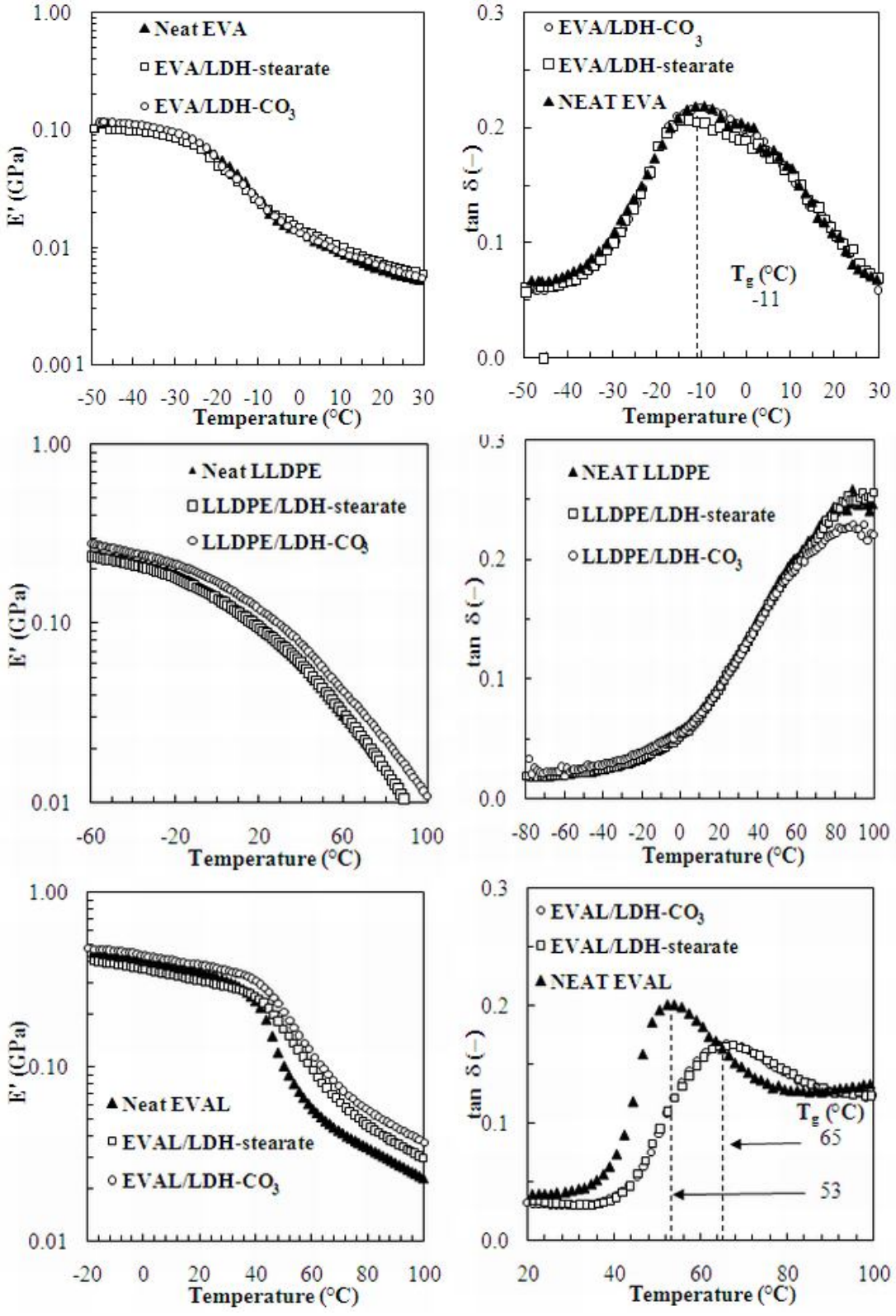

Figure C-4. Dynamic mechanical properties of 5% filler formulations

Mechanical Properties

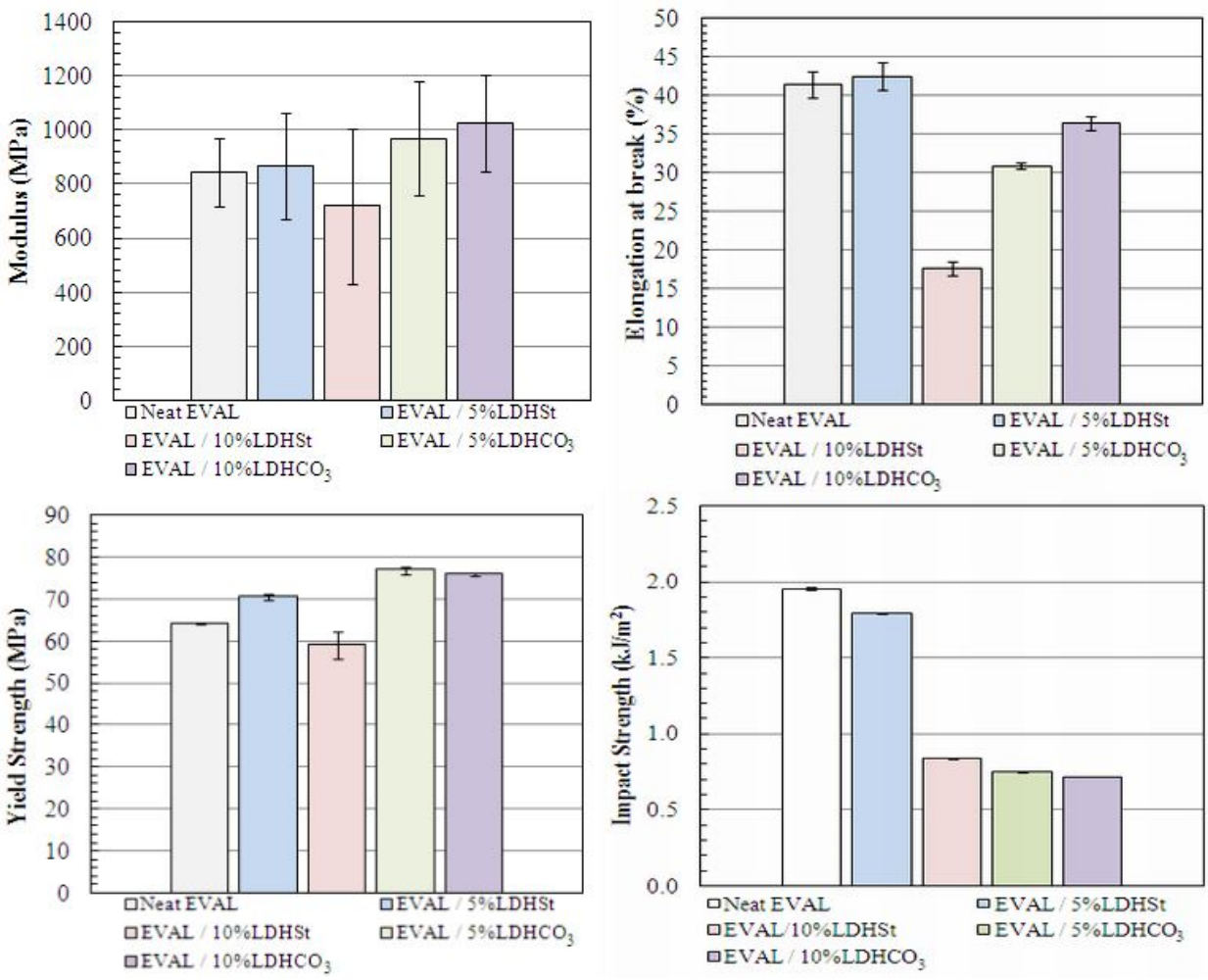

Figure C-5. Tensile strength and tensile impact test summary of neat EVAL and derivative composites

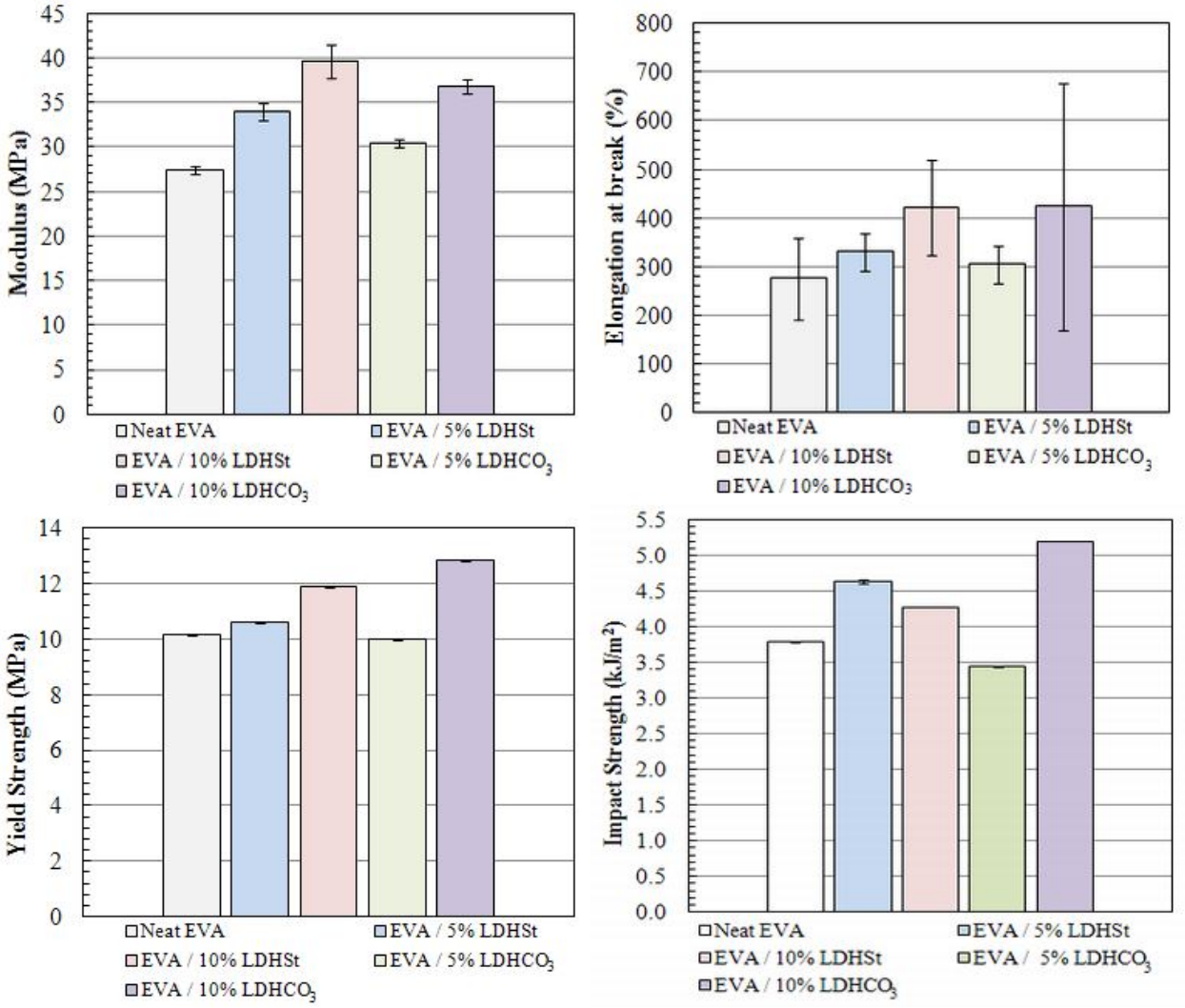

Figure C-6. Tensile strength and tensile impact test summary of neat EVA and derivative composites

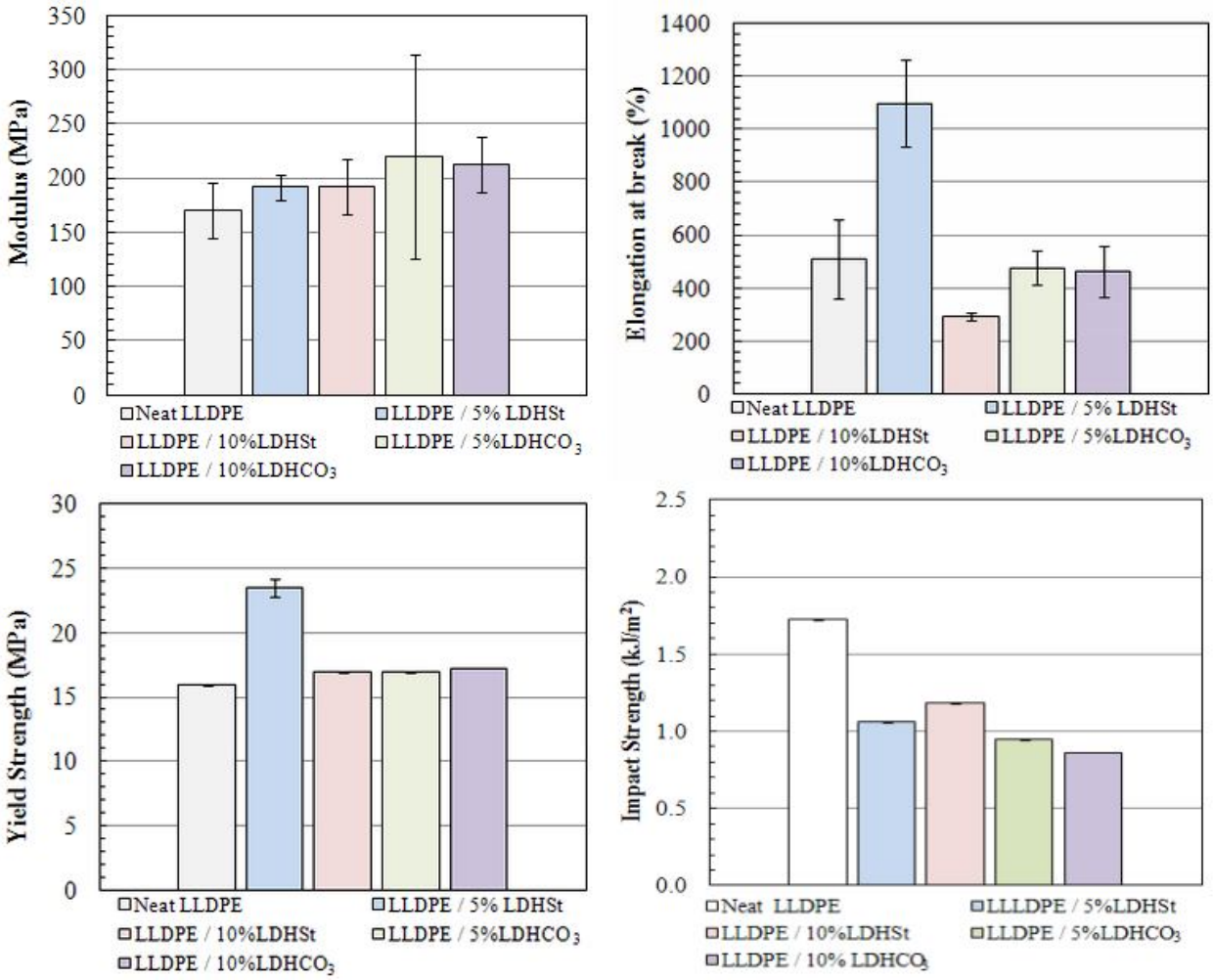

Figure C-7. Tensile strength and tensile impact test summary of neat LLDPE and derivative composites

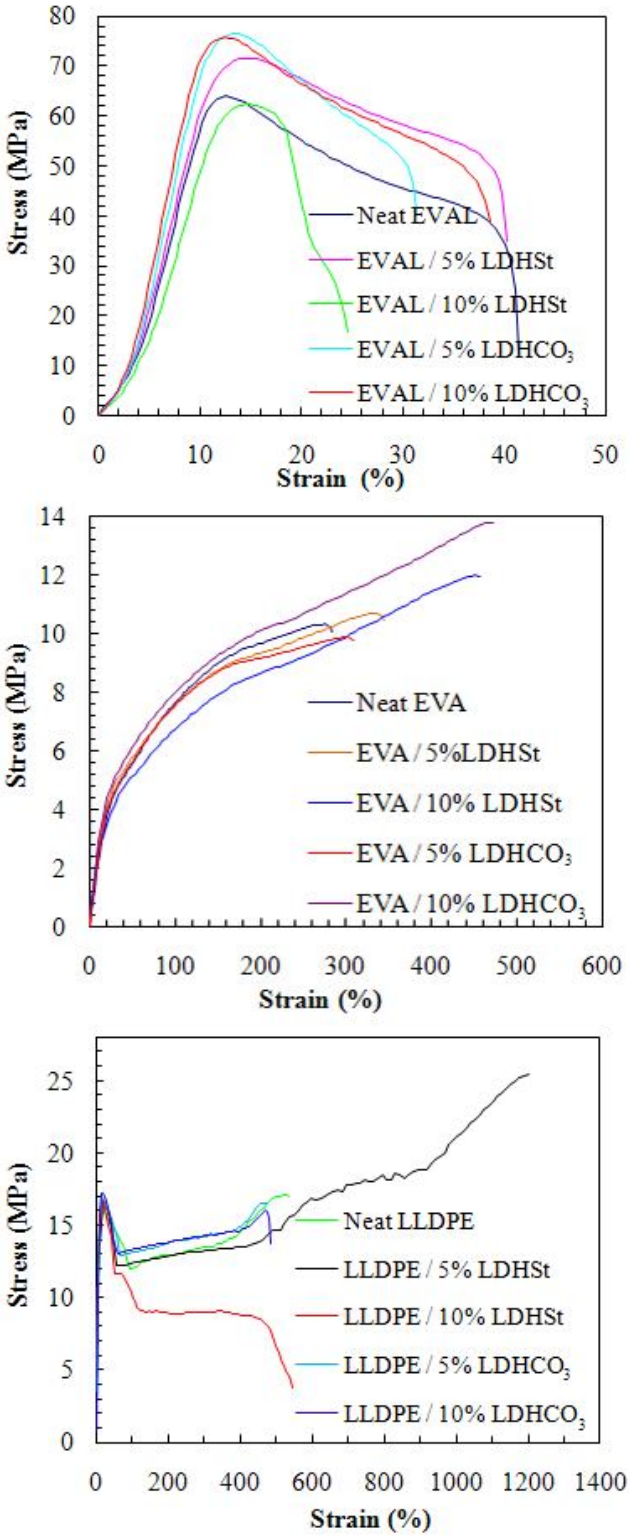

Figure C-8. Tensile test results

Fracture Behaviour

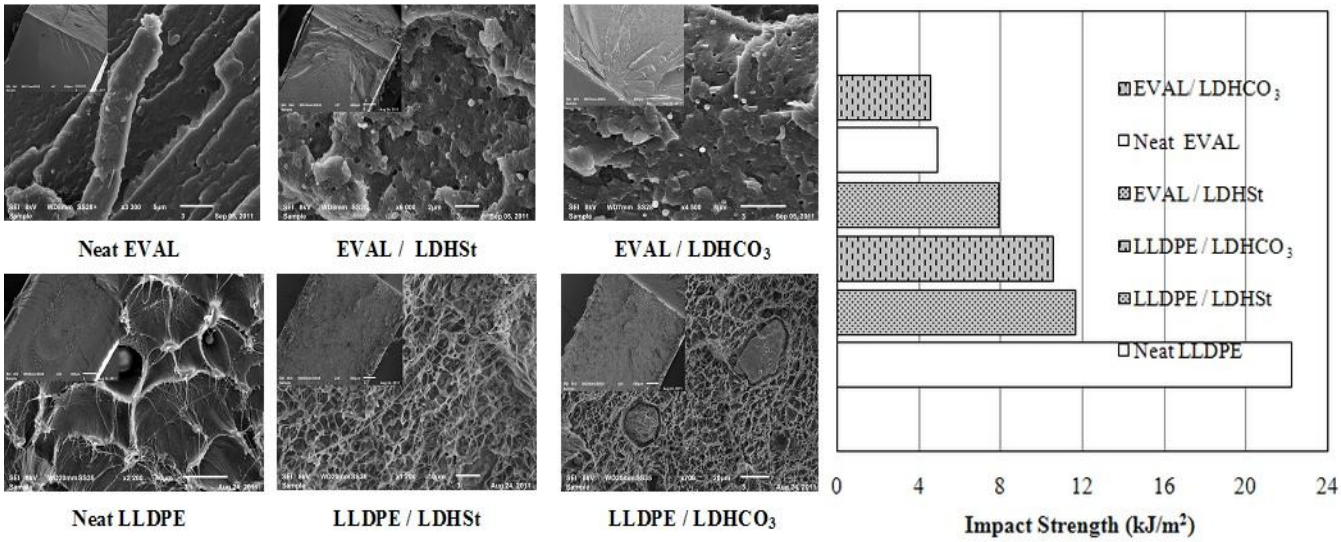

Figure C-9. SEM micrographs of fractured surfaces from the Charpy impact test and corresponding data (composites of 10 wt.% LDH)

Figure C-9 shows SEM micrographs of the Charpy impact specimens of the LDH/polymer composite samples. As mentioned earlier, breaks were observed in the EVAL and LLDPE samples. The two matrix systems show two different types of break, i.e. a brittle and a ductile break for the EVAL and LLDPE composites respectively. The EVAL specimens show a classic brittle break, with a mirror region extending radially outward from the initial flaw, forming a hackled region. Normally, fracture is perpendicular to polymer fibres, but angular cracks and breaks are observed in the composite samples. A closer look at the inserts of EVAL composites shows a granular fracture, implying that the addition of the LDH induces strong association within the polymer matrix. It is clear that the adhesion between the EVAL and the LDH is good as there is no clear distinction between the platelets and the polymer. The polymer continued to cover the LDH particles at the time of fracture.

DSC Data

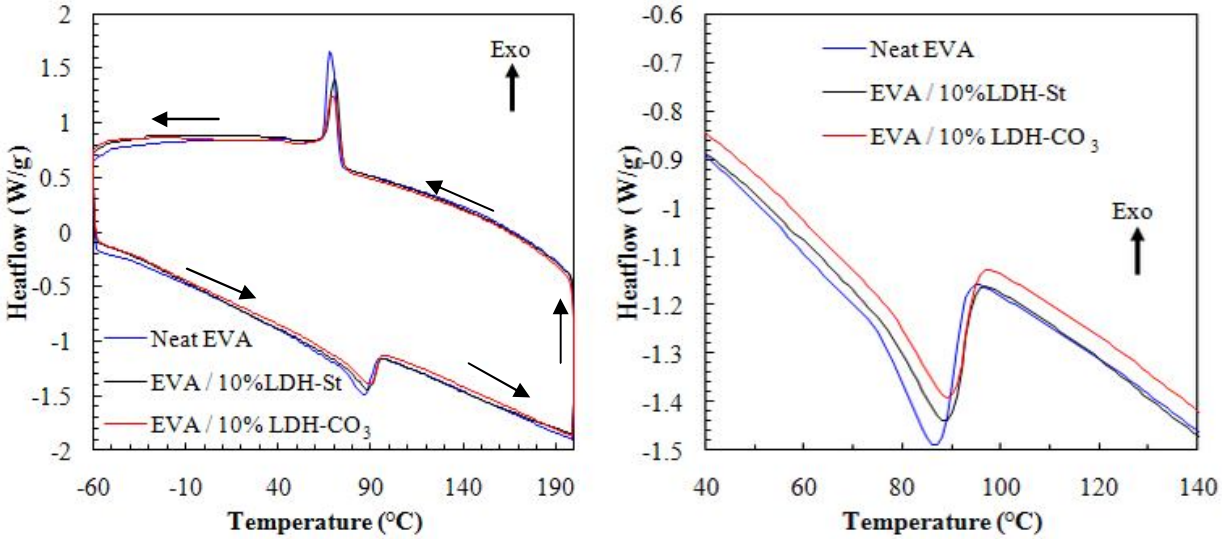

Figure C-10. DSC scans of EVA and derivative composites

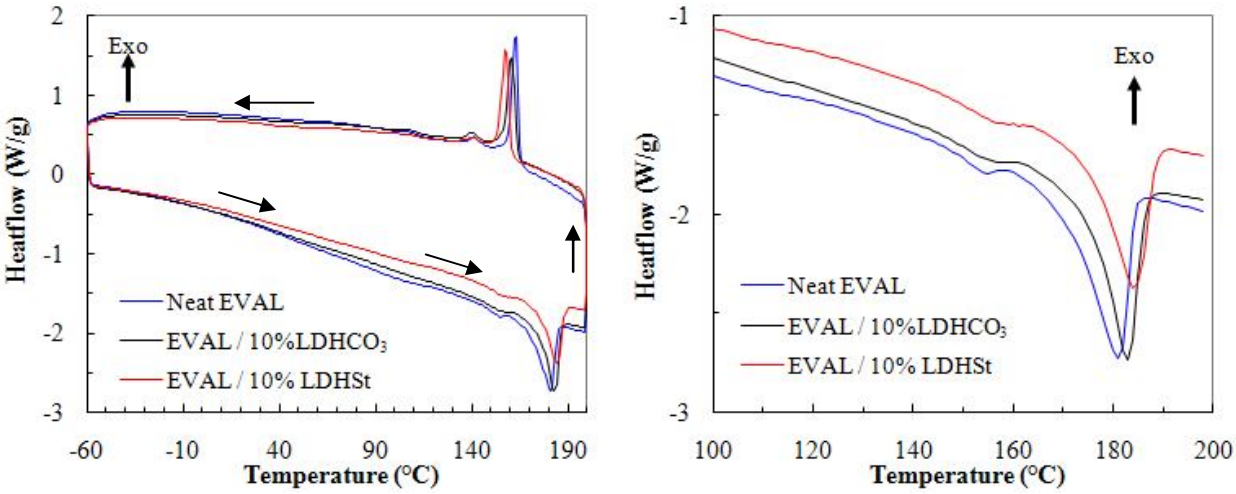

Figure C-11. DSC scans of EVAL and derivative composites

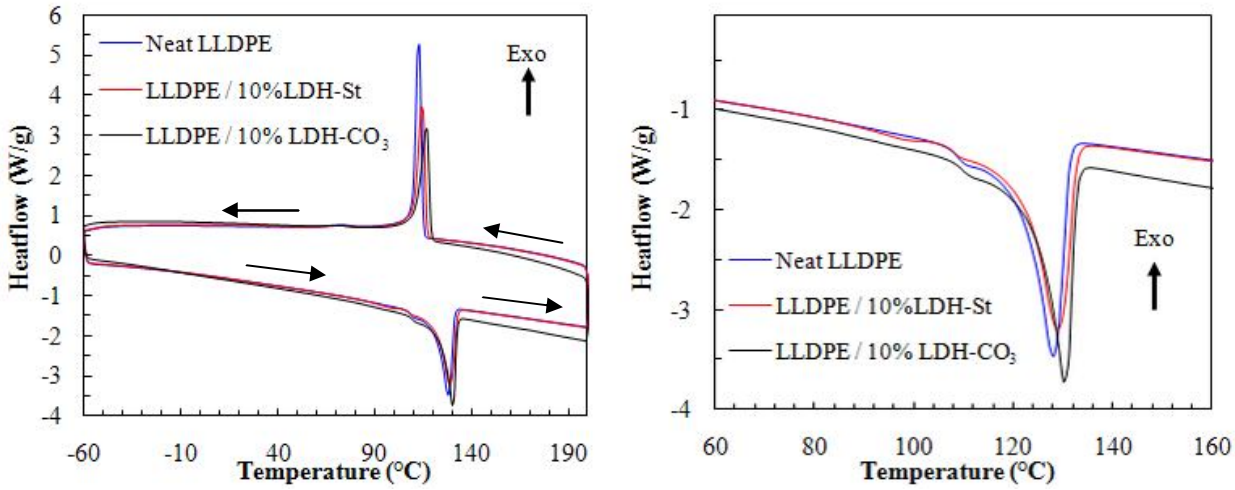

Figure C-12. DSC scans of LLDPE and derivative composites

The figures below are DSC scans of the 5% LDH loading. A slight change is observed in the melting and crystallisation temperatures of each of the filled systems.

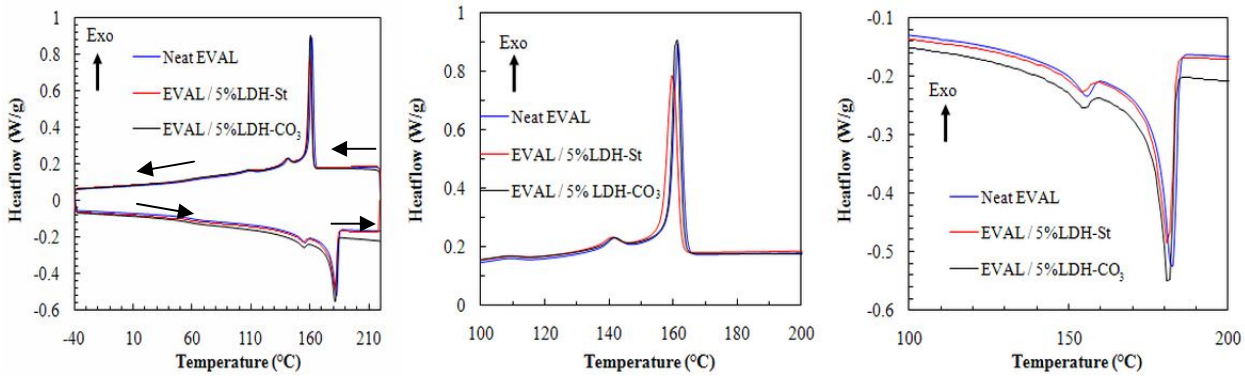

Figure C-13. DSC scans of EVAL and derivative composites

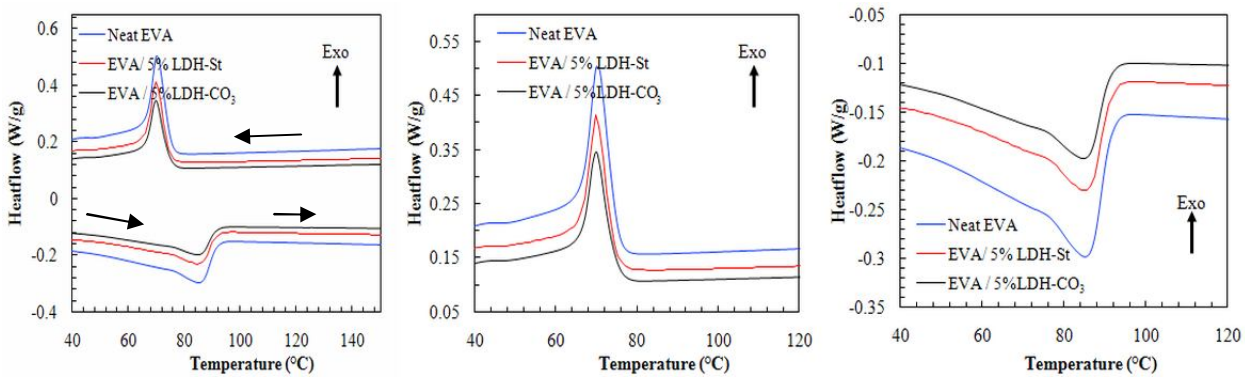

Figure C-14. DSC scans of EVA and derivative composites

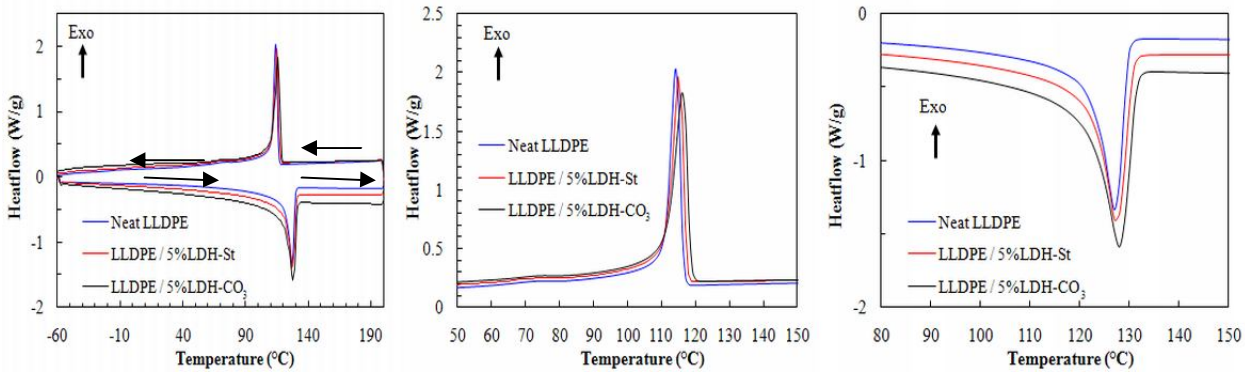

Figure C-15. DSC scans of LLDPE and derivative composites

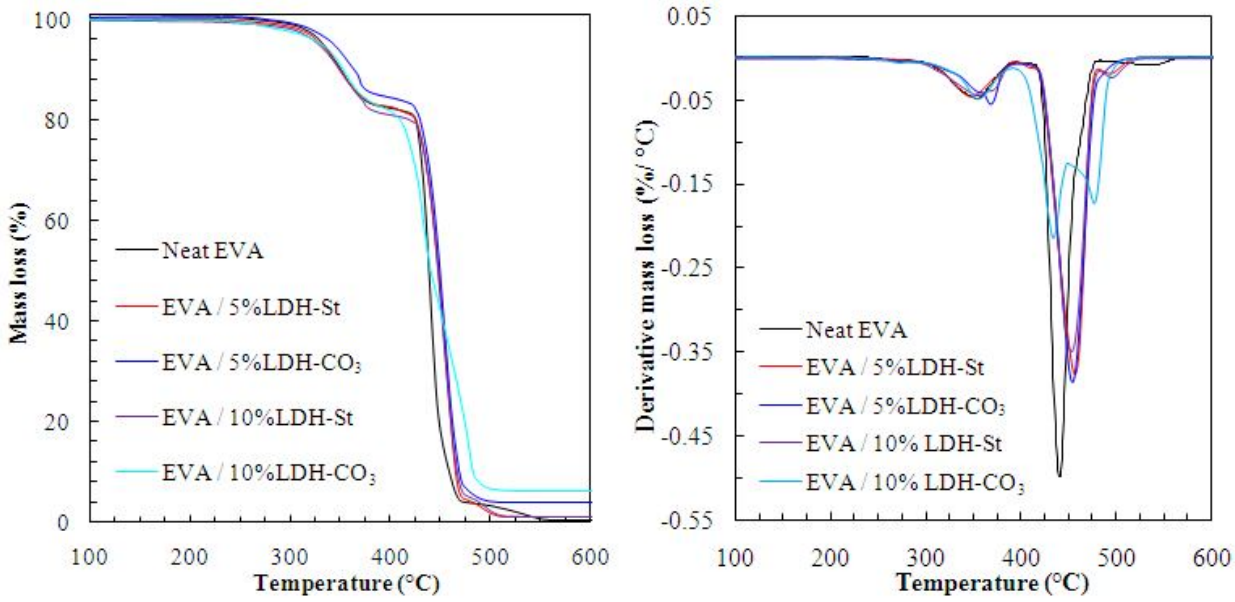

Figure C-16. TG data of EVA and derivative composites

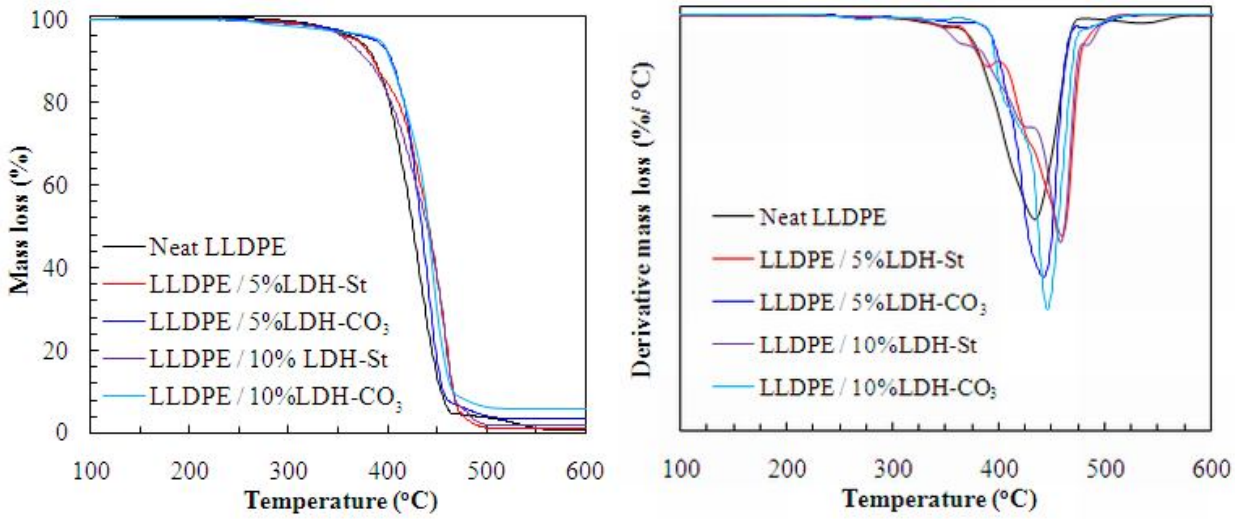

Figure C-17. TG data of EVA and derivative composites

Evolved Gas Analysis

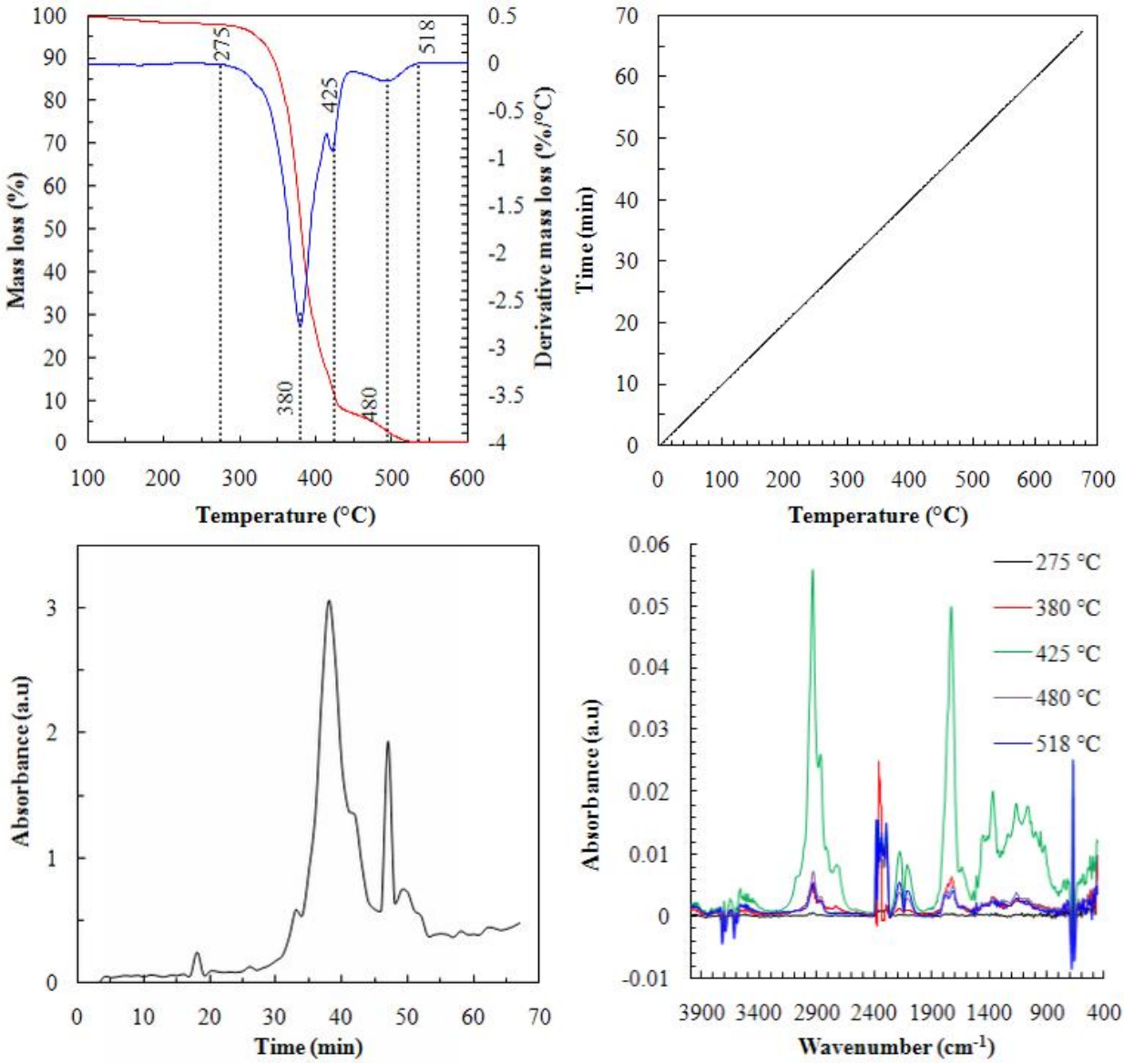

Figure C-18. Evolved gas analysis of neat EVAL by TG-FTIR

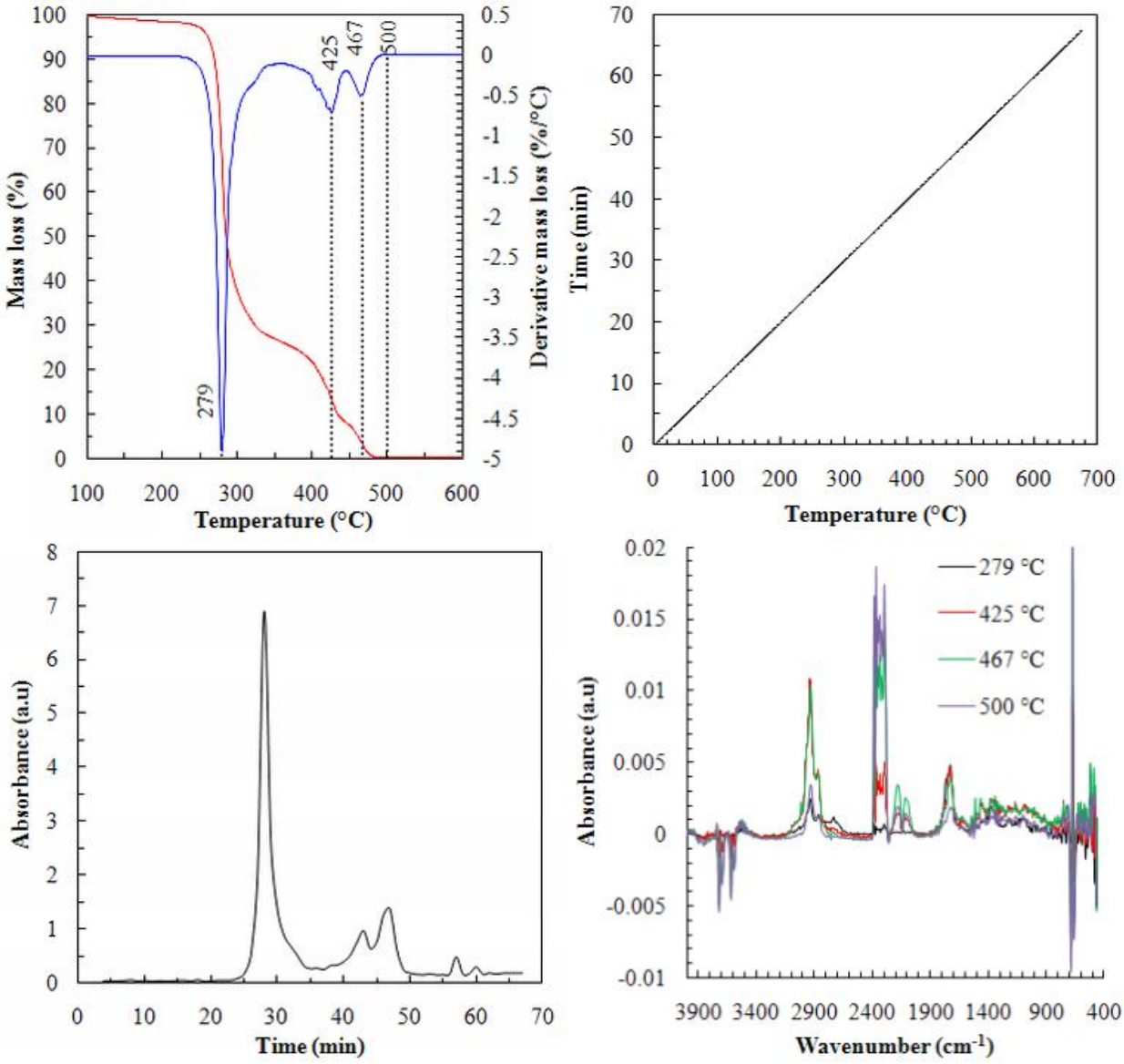

Figure C-19. Evolved gas analysis of EVAL/5% LDH-St by TG-FTIR

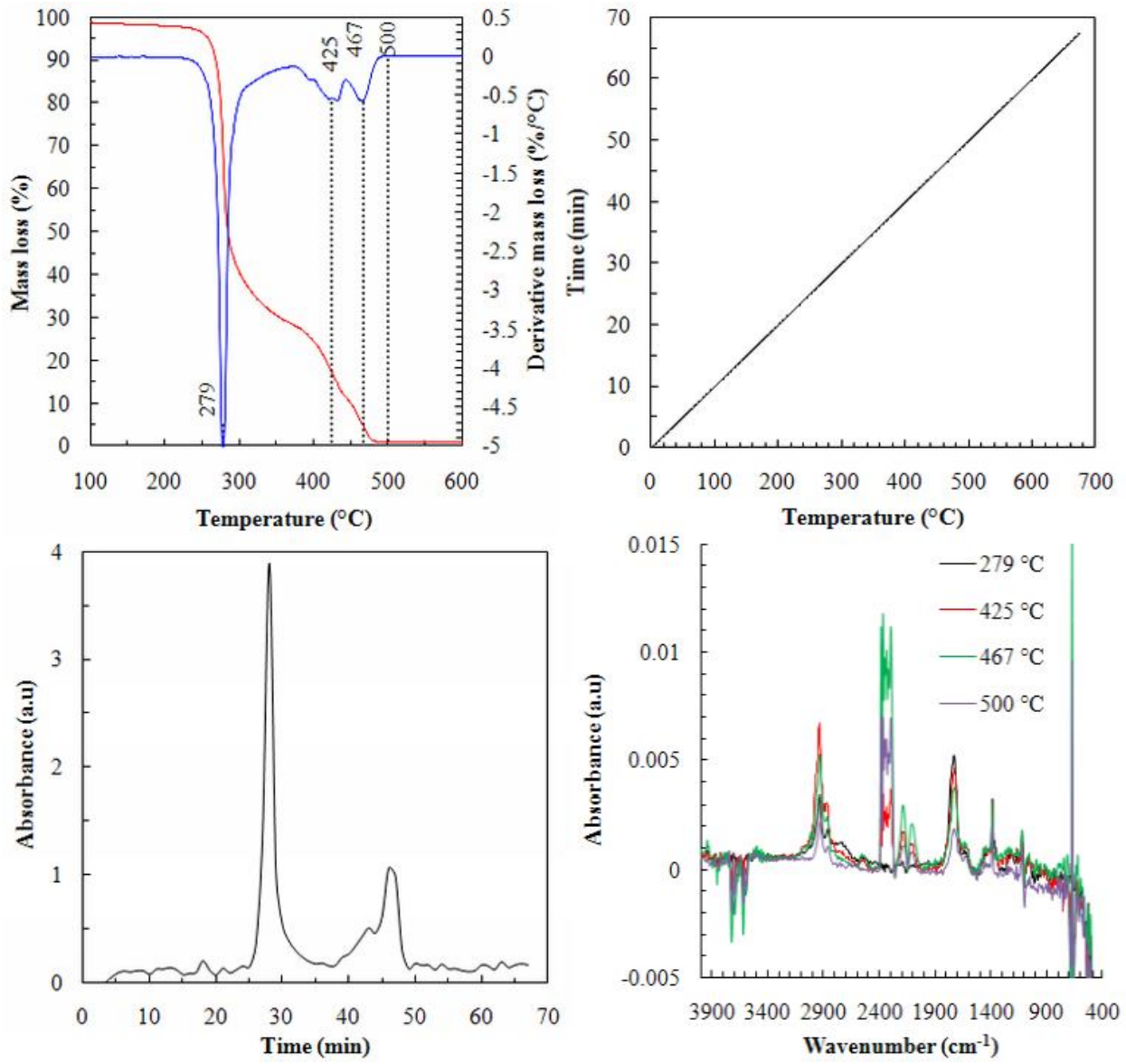

Figure C-20. Evolved gas analysis of EVAL/10% LDH-St by TG-FTIR

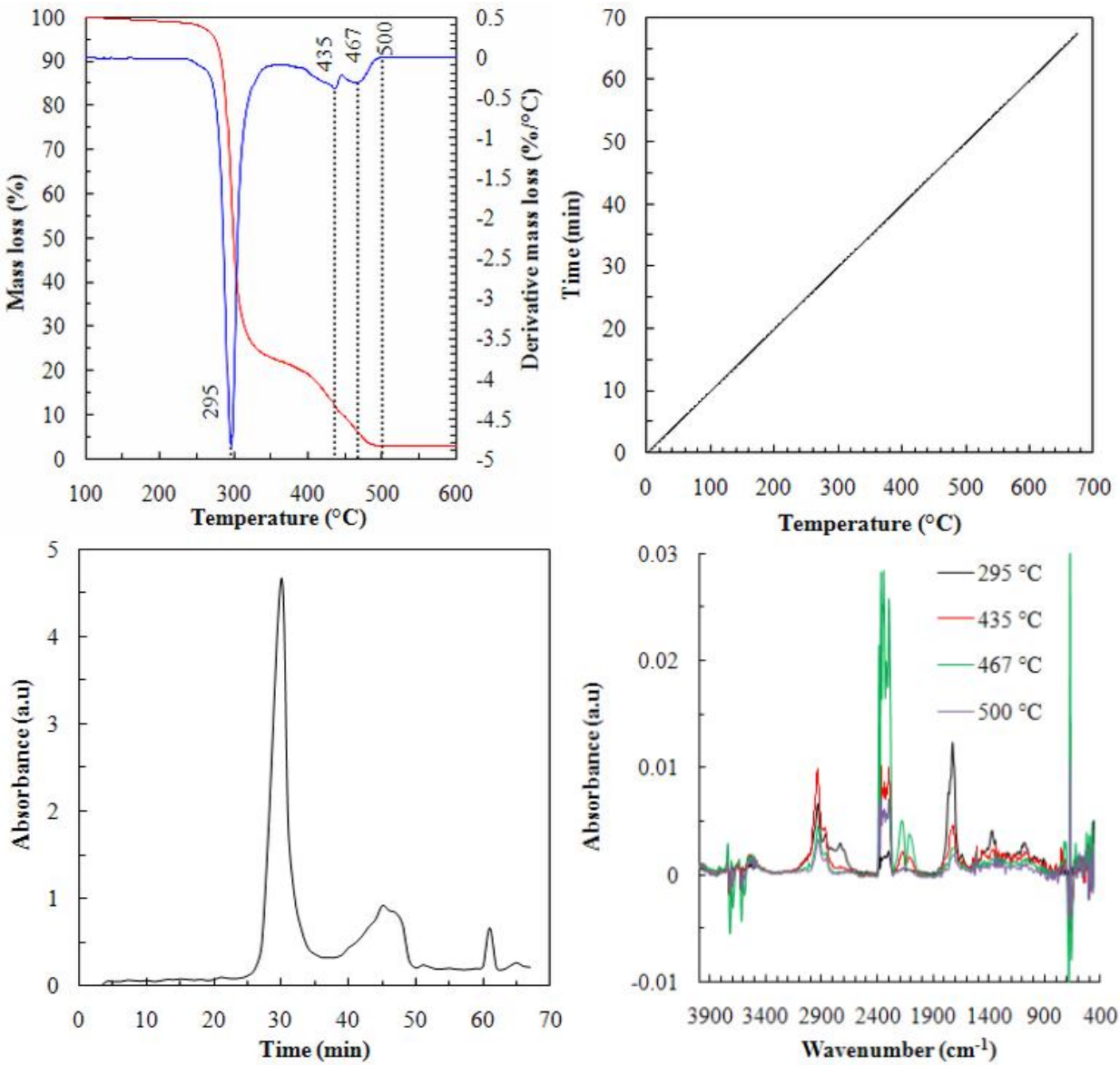

Figure C-21. Evolved gas analysis of EVAL/5% LDH-CO_3 by TG-FTIR

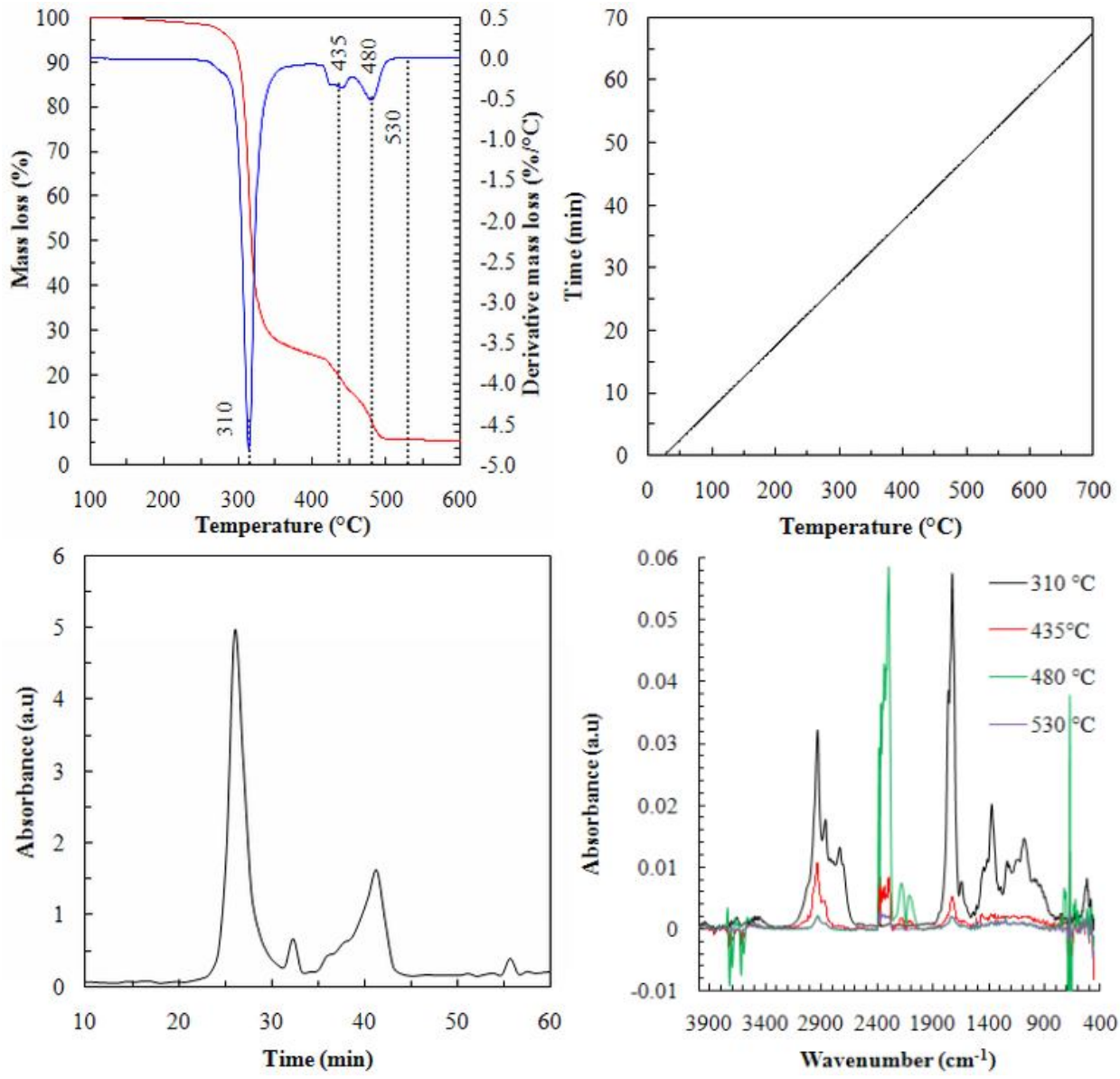

Figure C-22. Evolved gas analysis of EVAL/10% LDH-CO_3 by TG-FTIR

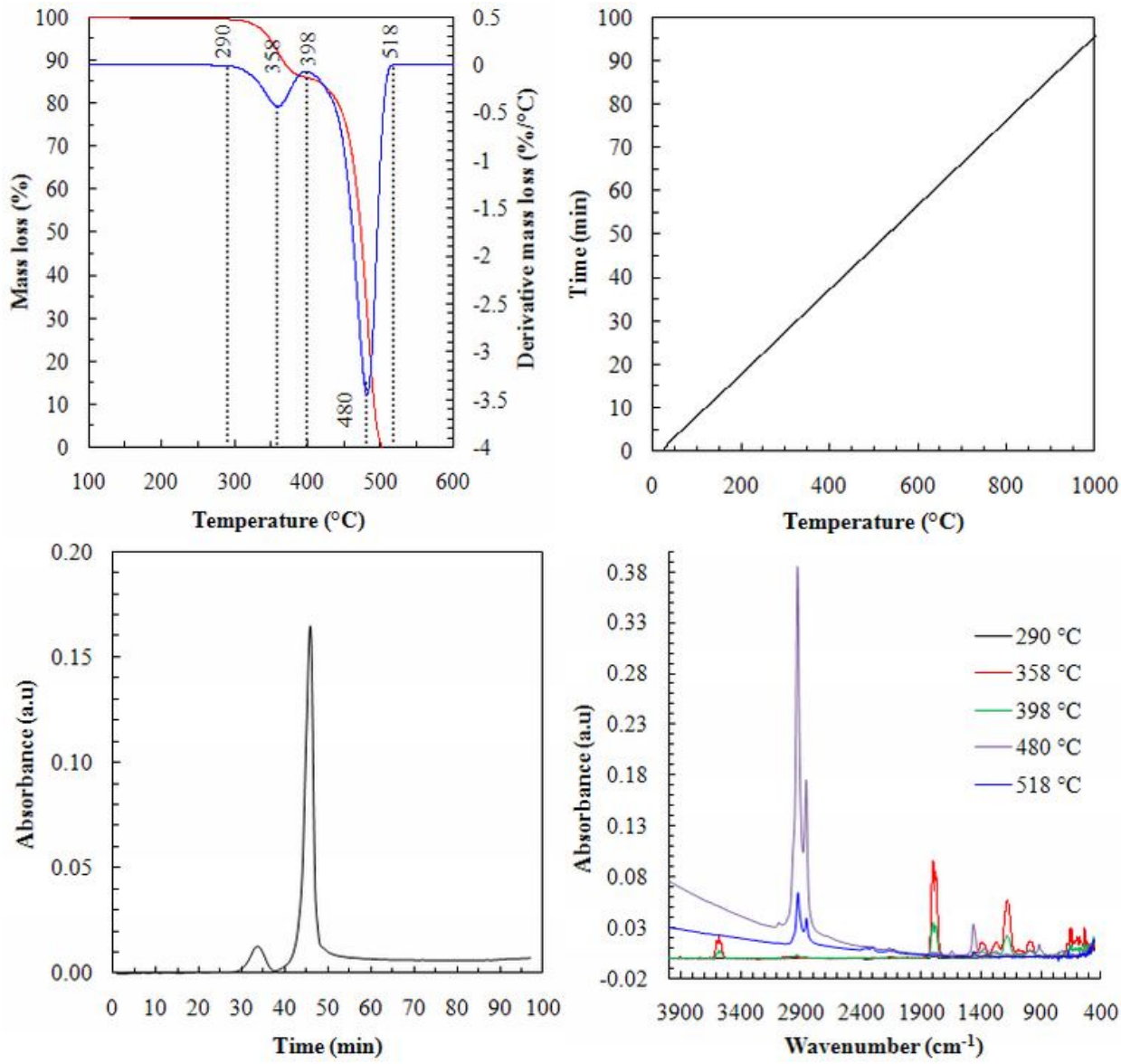

Figure C-23. Evolved gas analysis of neat EVA by TG-FTIR

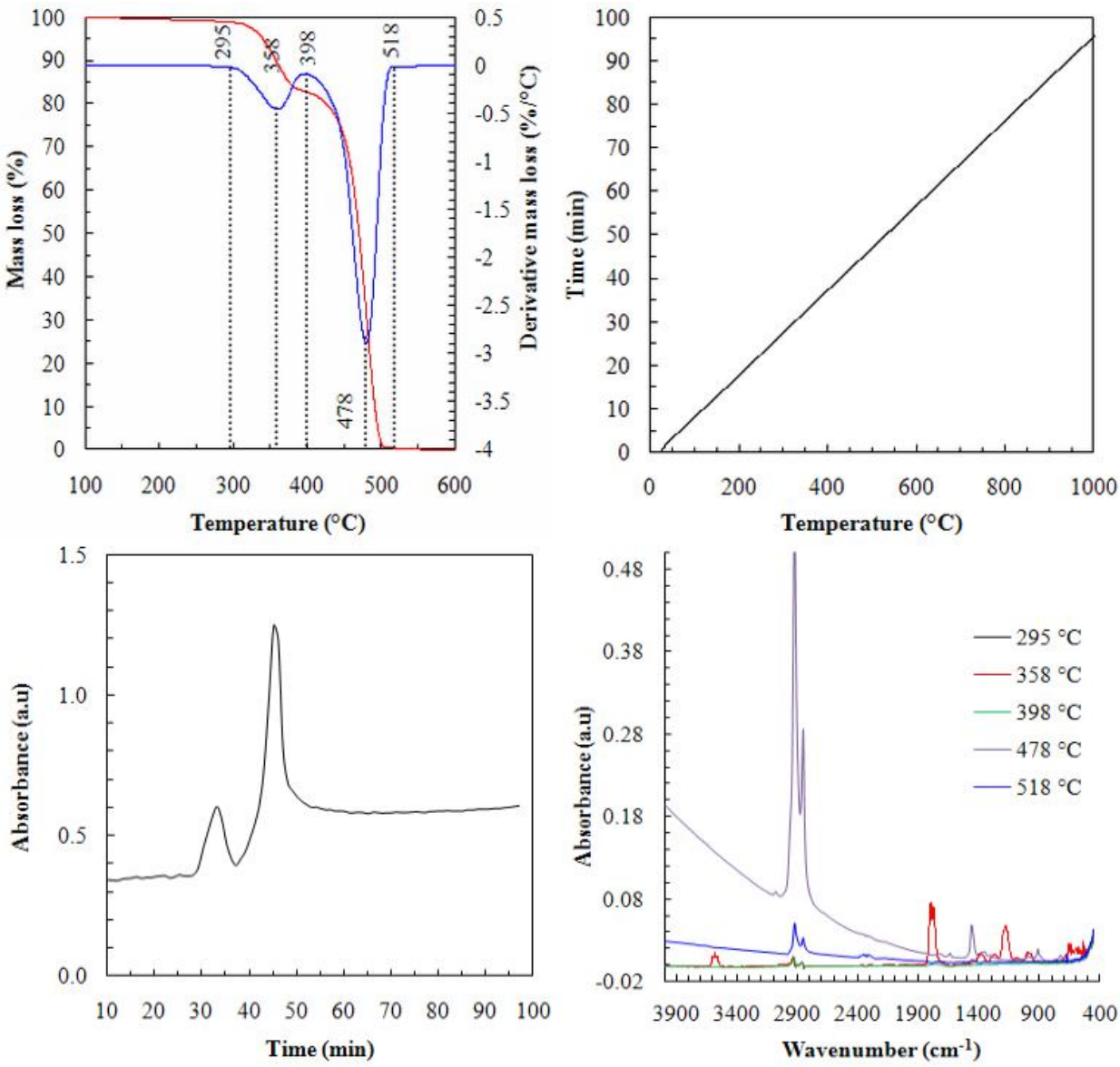

Figure C-24. Evolved gas analysis of EVA/5% LDH-St by TG-FTIR

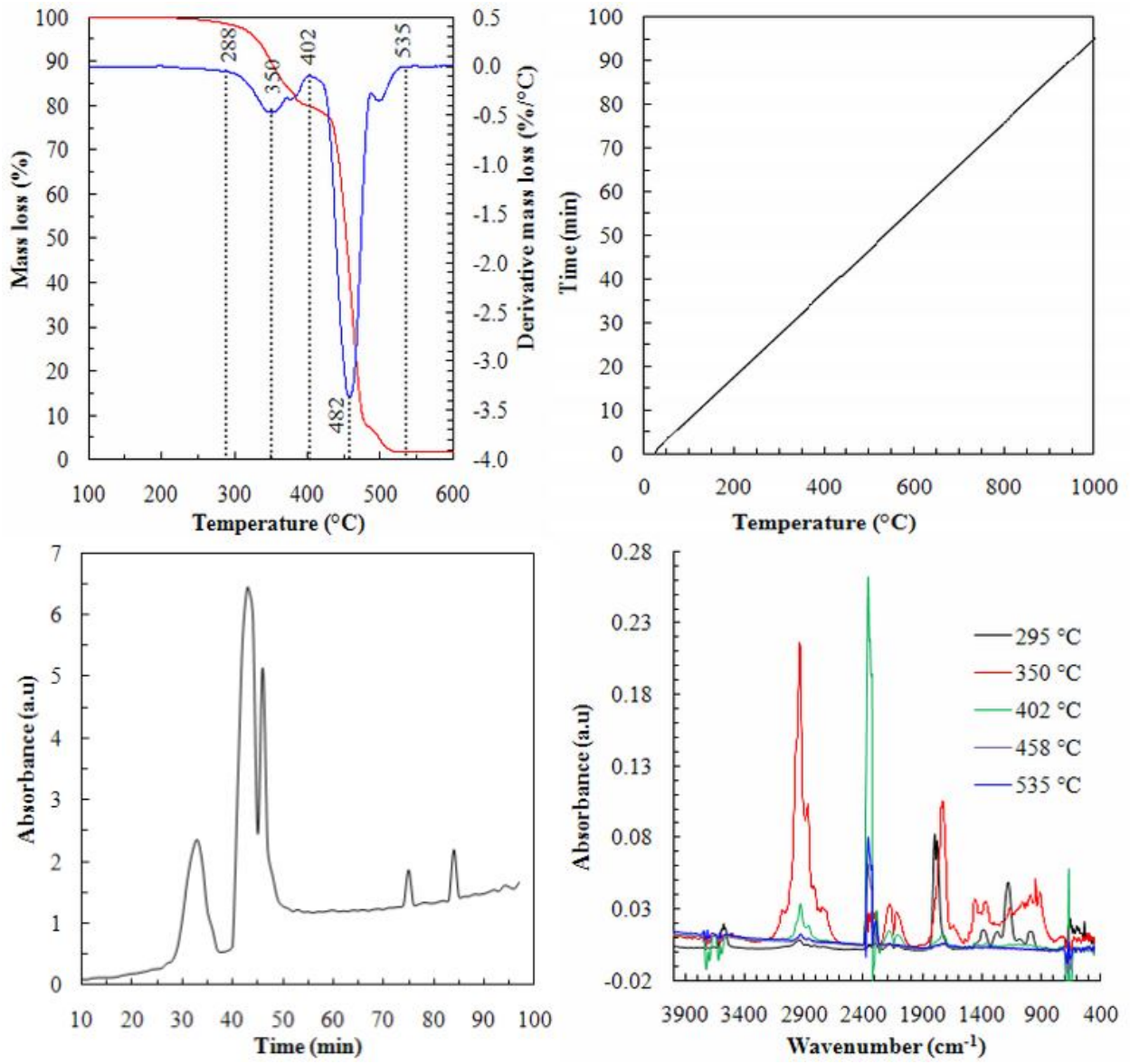

Figure C-25. Evolved gas analysis of EVA/10% LDH-St by TG-FTIR

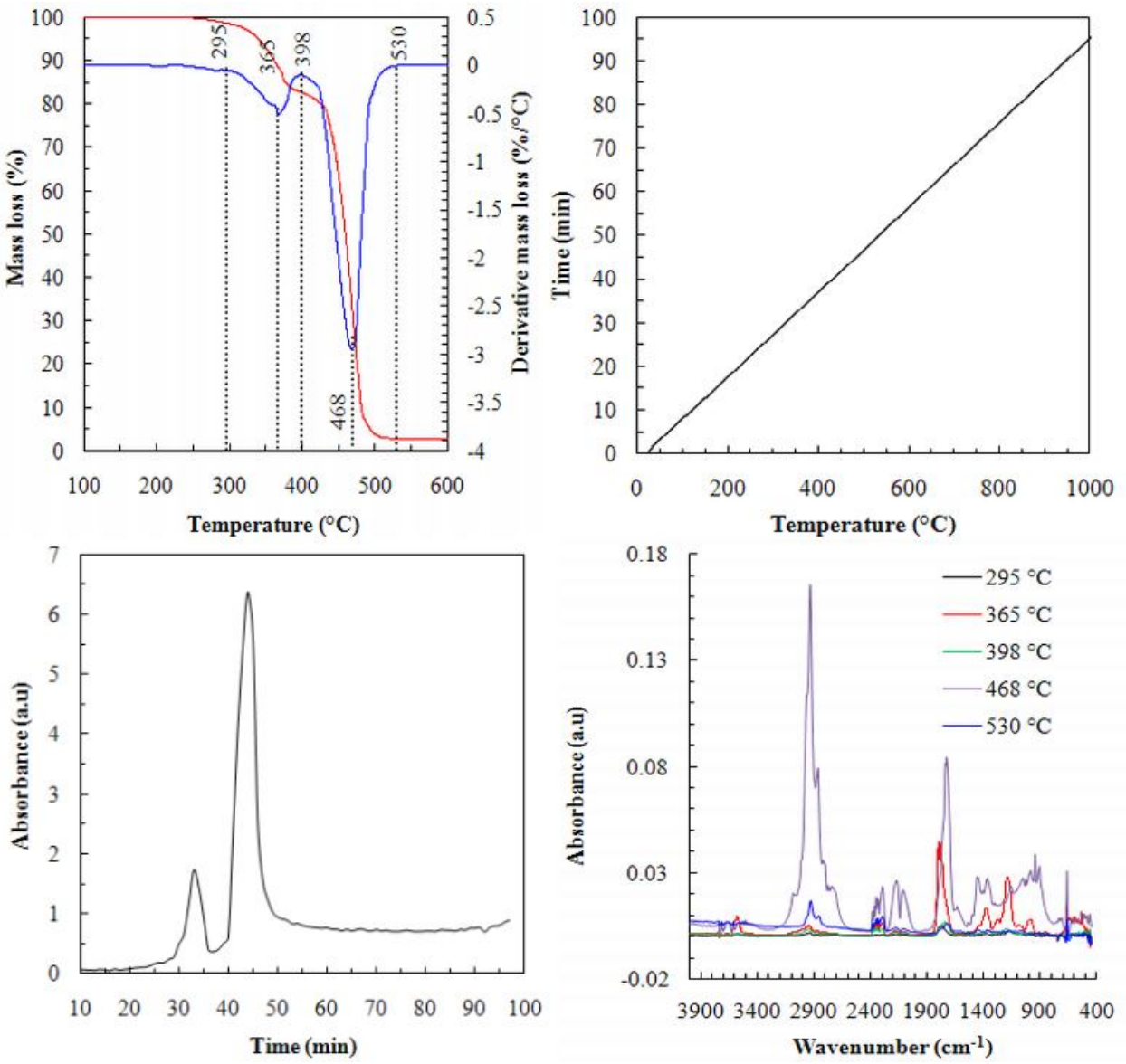

Figure C-26. Evolved gas analysis of EVA/5% LDH-CO_3 by TG-FTIR

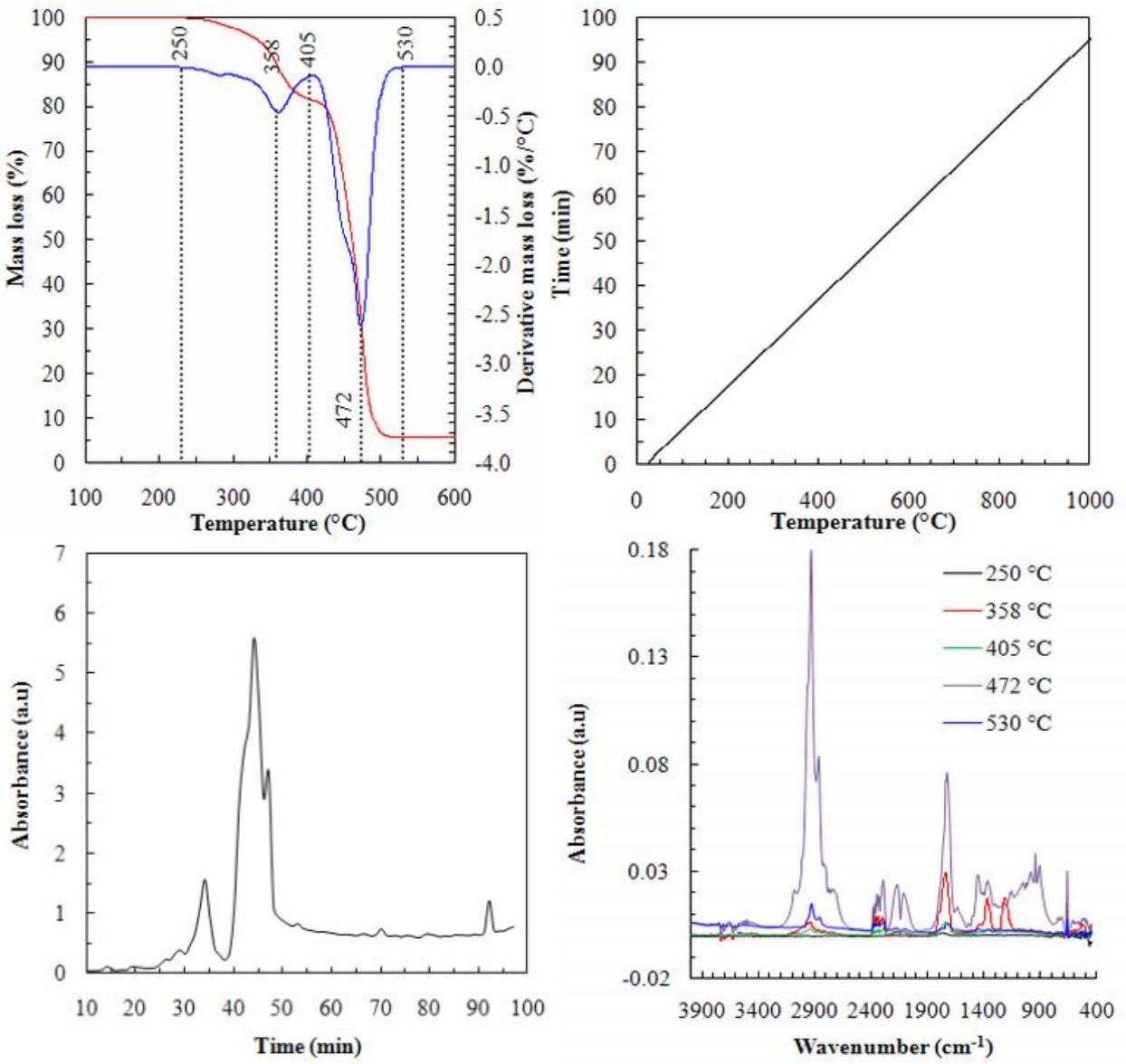

Figure C-27. Evolved gas analysis of EVA/10% LDH-CO_3 by TG-FTIR

Appendix D: Organo-LDH / Jojoba oil suspension

Fatty Acid-Jojoba Oil Formulation

Table D-1. Stearic acid in Jojoba oil formulation **(**J stands for Jojoba oil and S for stearic acid and their respective compositions**)**

Sample ID Formulation ratio	Weight of acid (g)	Weight of Jojoba oil (g)
J-S 95-5	0.5001	9.5028
J-S 90-10	1.004	9.0151
J-S 80-20	2.003	8.0044
J-S 70-30	3.007	7.0023

Table D-2. Palmitic acid in Jojoba oil formulation (J stands for Jojoba oil and P for palmitic acid and their respective compositions)

Sample ID Formulation ratio	Weight of acid (g)	Weight of Jojoba oil (g)
J-P 95-5	0.5003	9.5011
J-P 90-10	1.001	9.0034
J-P 80-20	2.009	8.0166
J-P 70-30	3.000	7.023

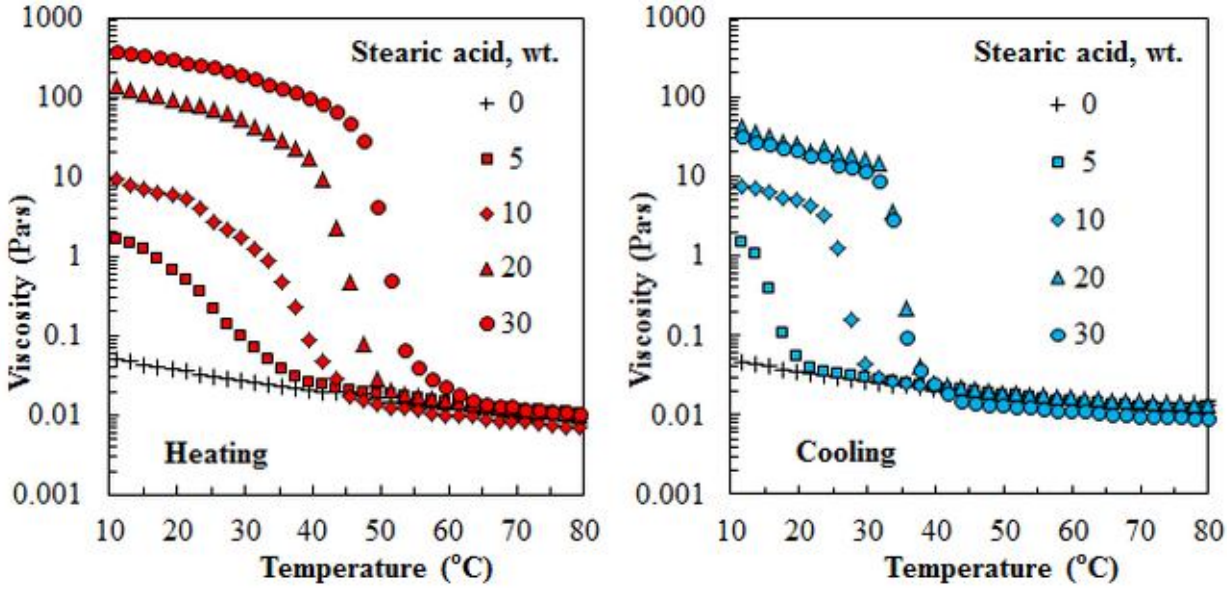

Figure D-1. Viscosity-temperature curve of different stearic acid compositions in Jojoba oil

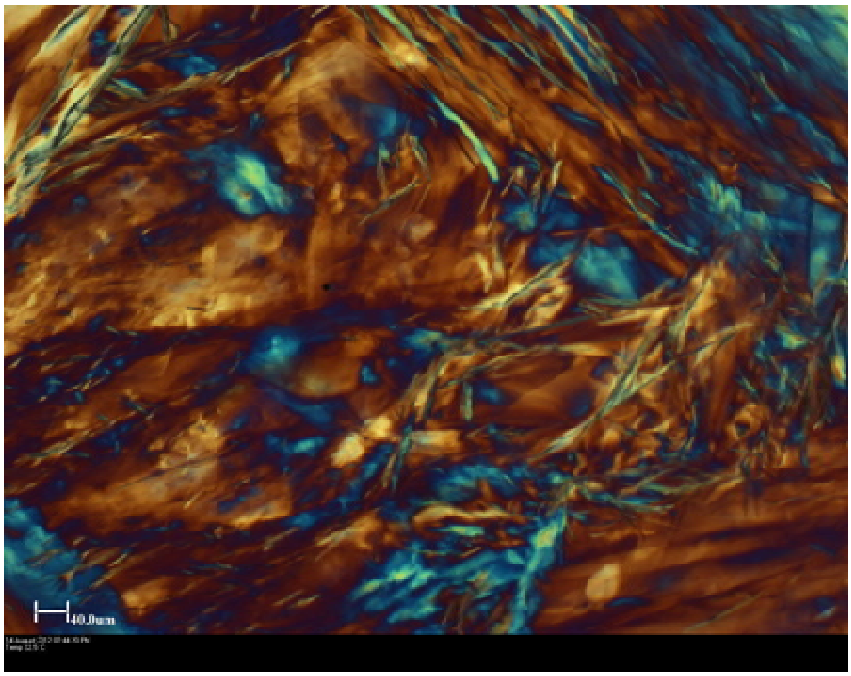

Figure D-2. 20 wt.% of stearic acid in Jojoba oil heated and cooled to 24 °C **(**measurement bar is 40 µm**)**

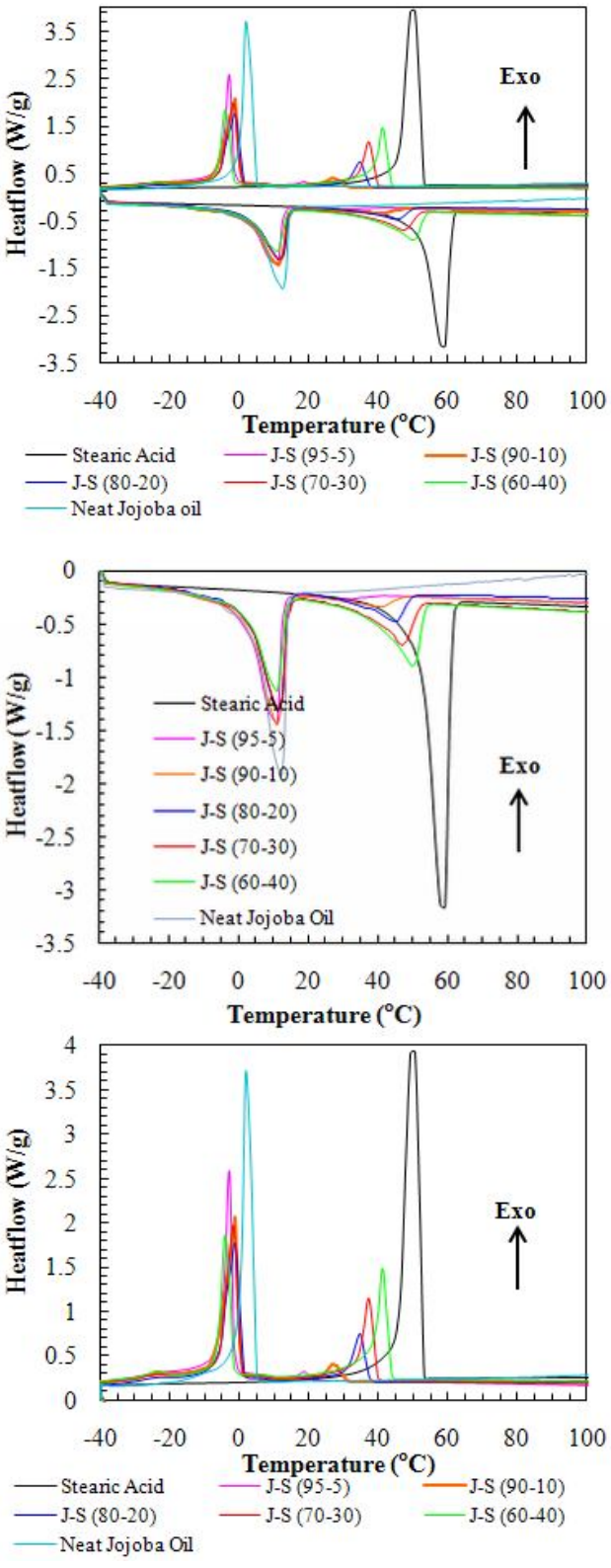

Figure D-3. DSC curves of different stearic acid compositions in Jojoba oil

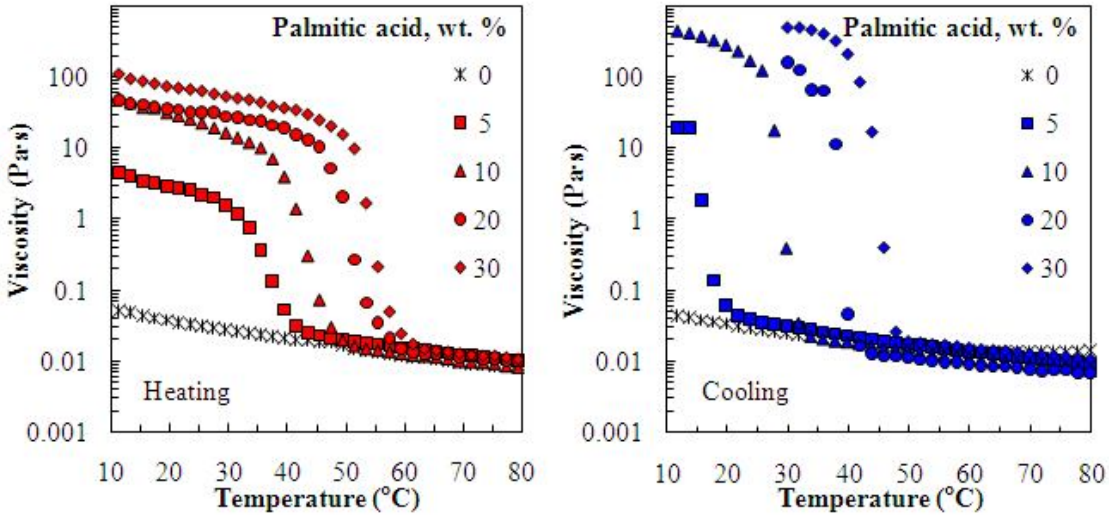

Figure D-4. Viscosity-temperature curve of different palmitic acid compositions in Jojoba oil

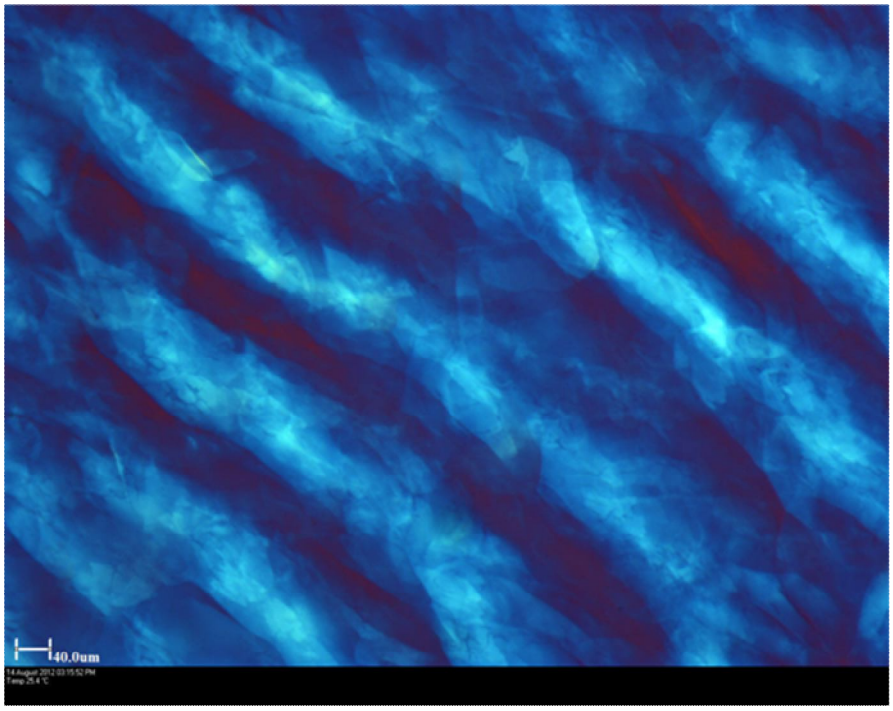

Figure D-5. 20 wt.% palmitic acid in Jojoba oil heated and cooled to 25 °C **(**measurement bar is 40 µm**)**

It is interesting to note that fatty acid crystallisation behaviour in Jojoba oil differs for stearic and palmitic acid. This could also explain the different gels obtained from the LDH-stearate and from the LDH-palmitate. Crystal shape, size and density were found to affect the physical properties of the final solid fat matrix (Rye *et al.*, 2005)

FT-IR Spectra

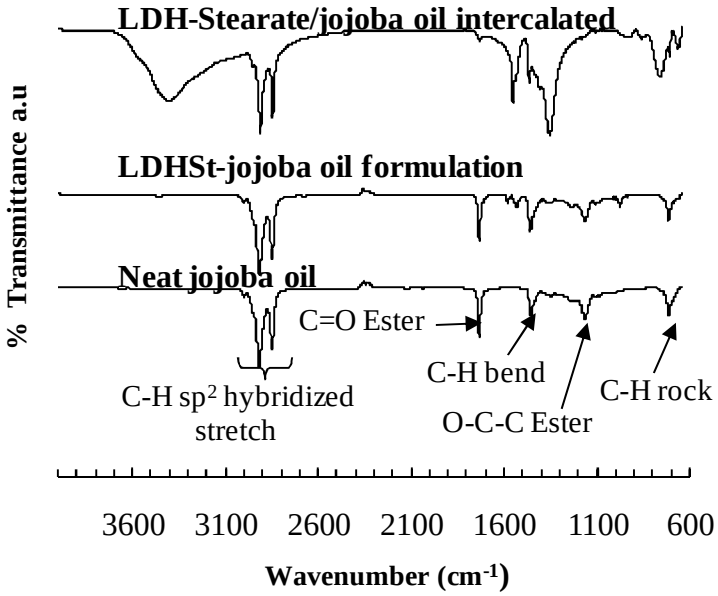

Figure D-6. FTIR spectra of **n**eat Jojoba oil, 30 wt.% LDH-stearate/Jojoba oil formulation and stearate

The Jojoba oil peaks are the same as those observed in Le Dreau *et al.*, 2008.

Rheology of Fatty Acid-Intercalated LDH/Jojoba Oil Formulation

Table D-3. Visual observation of different 30 wt% of intercalated LDHs

Sample ID	Carbon chain number	Orientation of intercalated anion	Appearance: unheated treated formulation	Appearance: heated treated formulation
LDH-myristate	C_{14}	Bilayer	Runny	Thickens slightly on standing
LDH-palmitate	C_{16}	Bilayer	Slightly runny	Thickens slightly on standing
LDH-stearate	C_{18}	Bilayer	Dropping consistency	Thickens slightly on standing
LDH-oleate	C_{18}	Bilayer	Runny	No change
LDH-behenate	C_{22}	Bilayer	Soft dropping consistency	Thickens slightly on standing

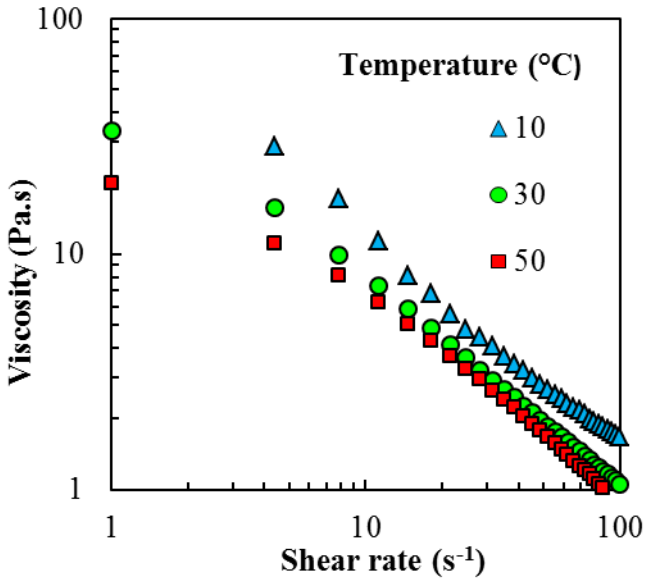

Figure D-7. The effect of shear rate and temperature on the viscosity of Jojoba oil suspensions **(**the LDH-stearate content was 30 wt.% and the shear rate was kept constant at 5 s^{-1}**)**

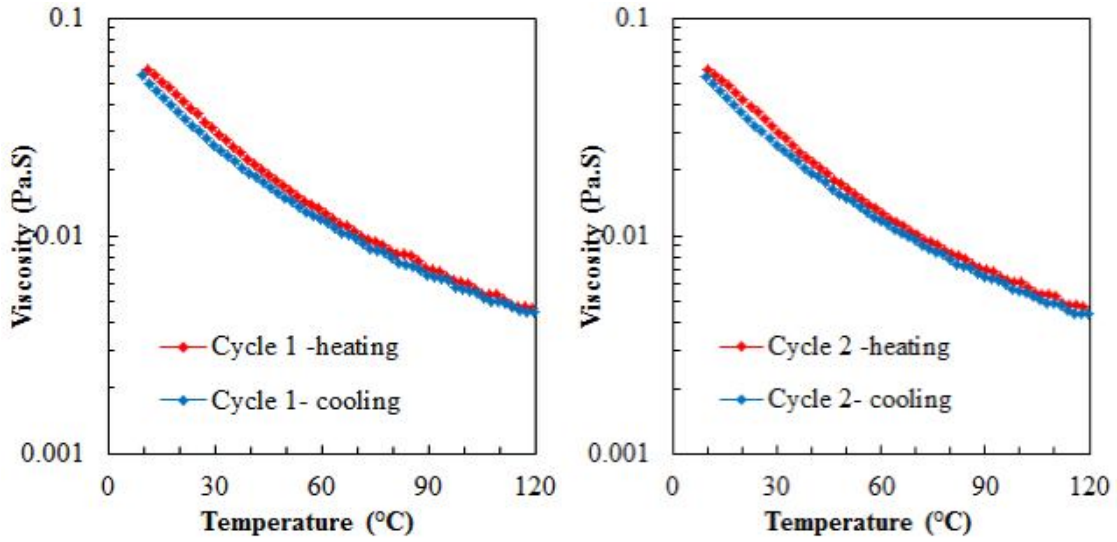

Figure D-8. Viscosity as a function of temperature of the neat Jojoba oil

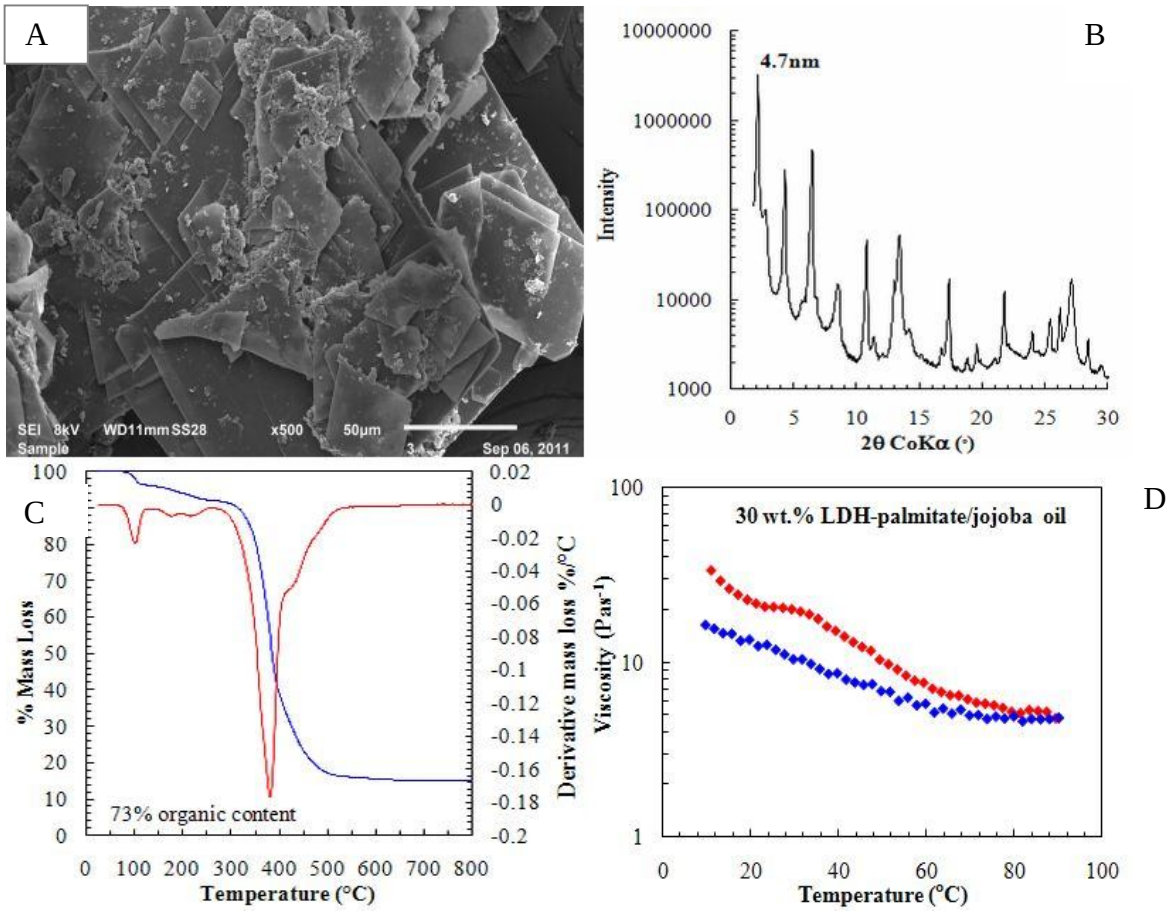

Figure D-9. Summary of rhombohedral-shaped LDH-palmitate**:** A – SEM image of morphology of particles**;** B **–** XRD diffractograms with a d-spacing of 4.7 nm**;** C **–** TGA data indicating organic content**;** D **– v**iscosity curve as a function of temperature of the derivative 30 wt.% formulation

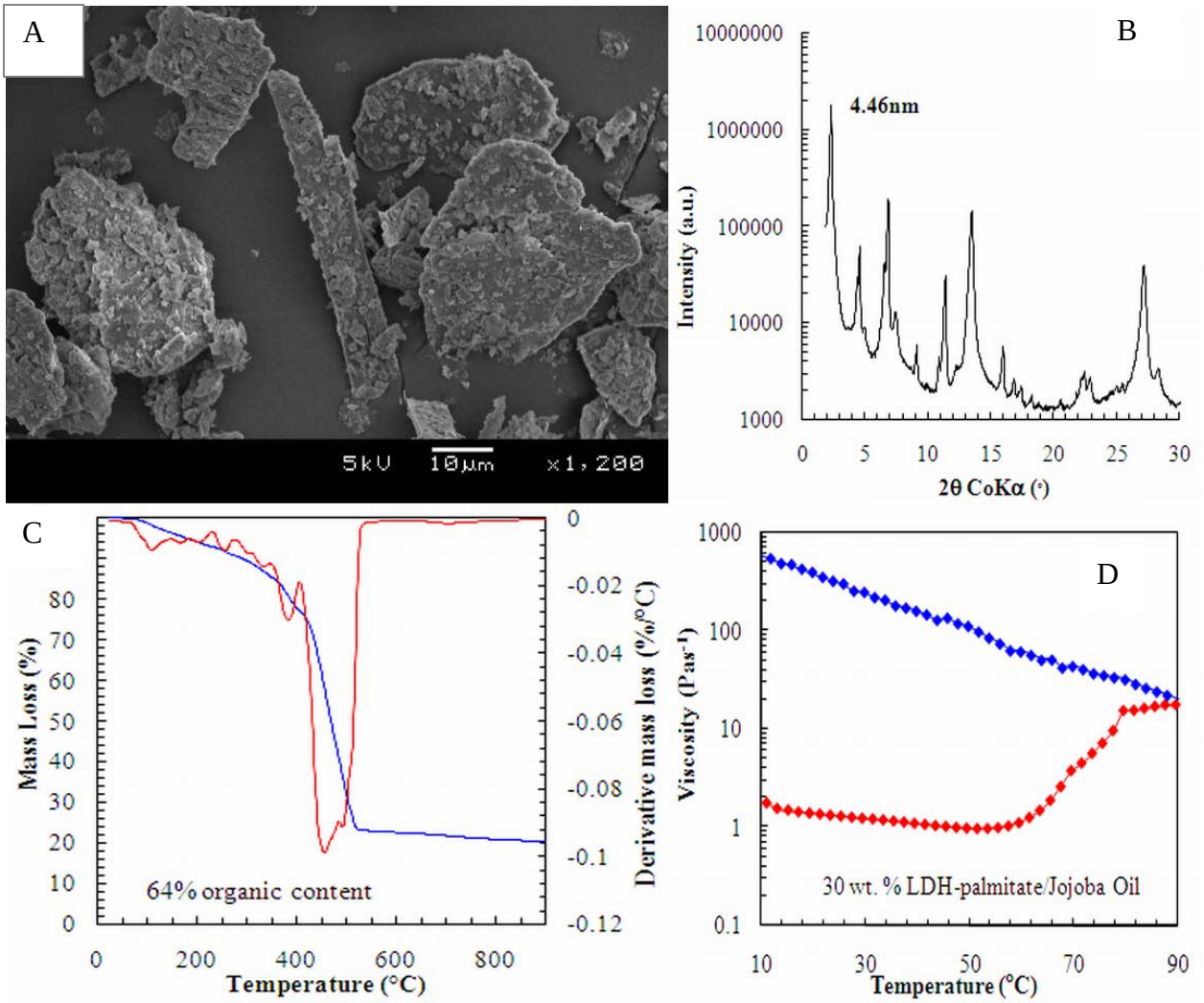

Figure D-10. Summary of subhedral-shaped LDH-palmitate**:** A – SEM image of morphology of particles**;** B – XRD diffractograms with a d-spacing of 4.46 nm**;** C – TGA data indicating organic content**;** D – **v**iscosity curve as a function of temperature of the derivative 30 wt.% formulation

Complex viscosity behaviour was observed for the C_{16}–C_{22} intercalated LDHs.

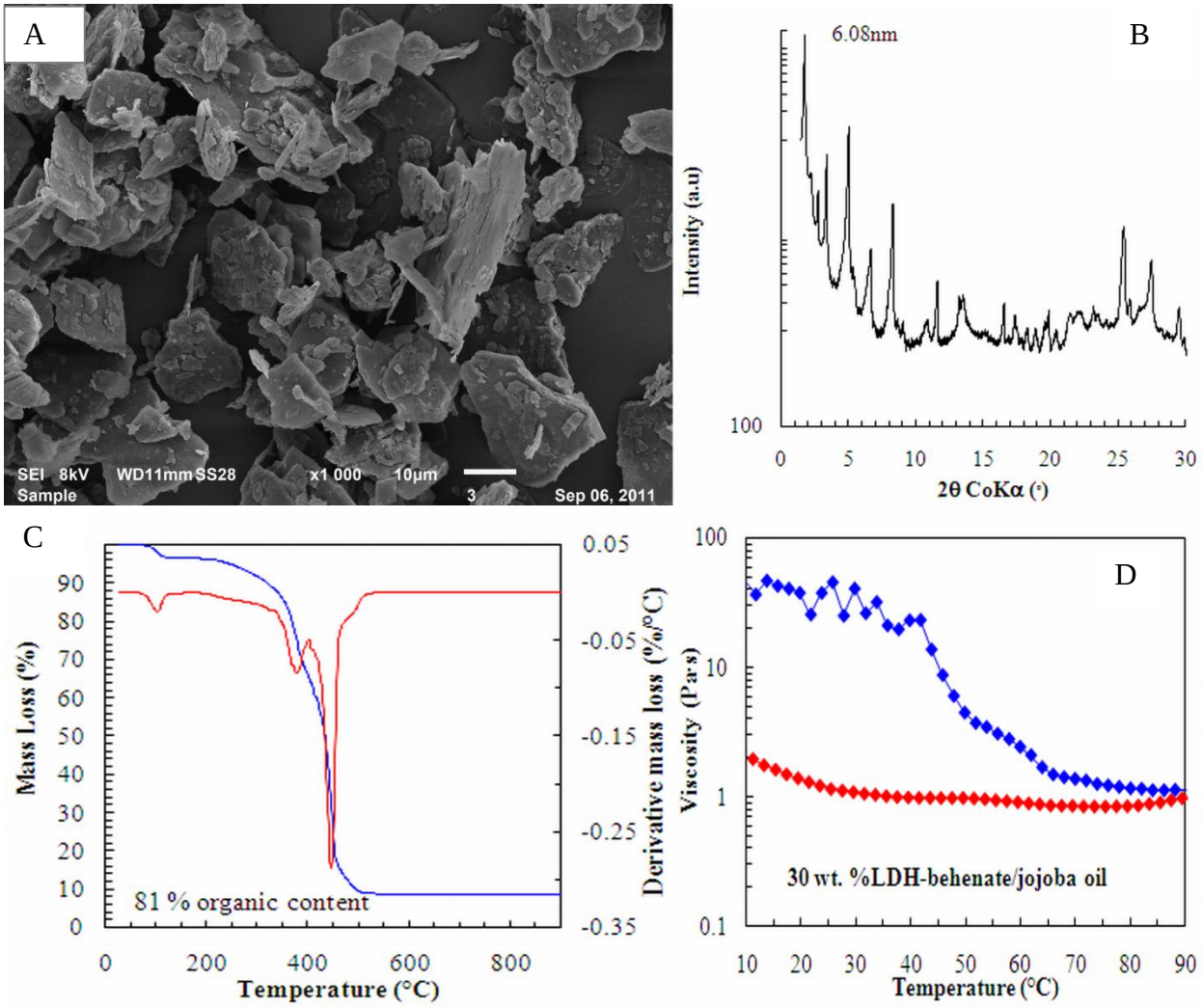

Figure D-11. Summary of subhedral-shaped LDH-behenate**:** A – SEM image of morphology of particles**;** B **–** XRD diffractograms with a d-spacing of 6.08 nm**;** C **–** TGA data indicating organic content**;** D **– v**iscosity curve as a function of temperature of the derivative 30 wt.% formulation

Other formulations were attempted with LDH-palmitate and behenate/Jojoba oil systems, and similar results were obtained. However, the products were found to have a higher viscosity that the LDH-stearate derivatives and became grease-like. This could be explained by the fatty acid-platelet association, which results in the release of a hydrogen ion (H^+). The hydrogen attacks the unsaturated bonds of the Jojoba oil. Hydrogenation of these bonds

results in the change of properties from oil (liquid) to wax (solid-like). Hence, fatty acid-intercalated LDHs may potentially be used as rheological modifiers. As a result it is recommended that further analysis and experimentation be conducted to determine the effect that LDH-fatty acid has on the rheological behaviour of Jojoba oil.

The co-intercalated samples also showed this complex viscosity, i.e. for the palmitic and stearic acid co-intercalated LDH (LDH-Pal-St), and for the Jojoba oil and stearic acid-intercalated LDH (LDH-Jojoba/stearate).

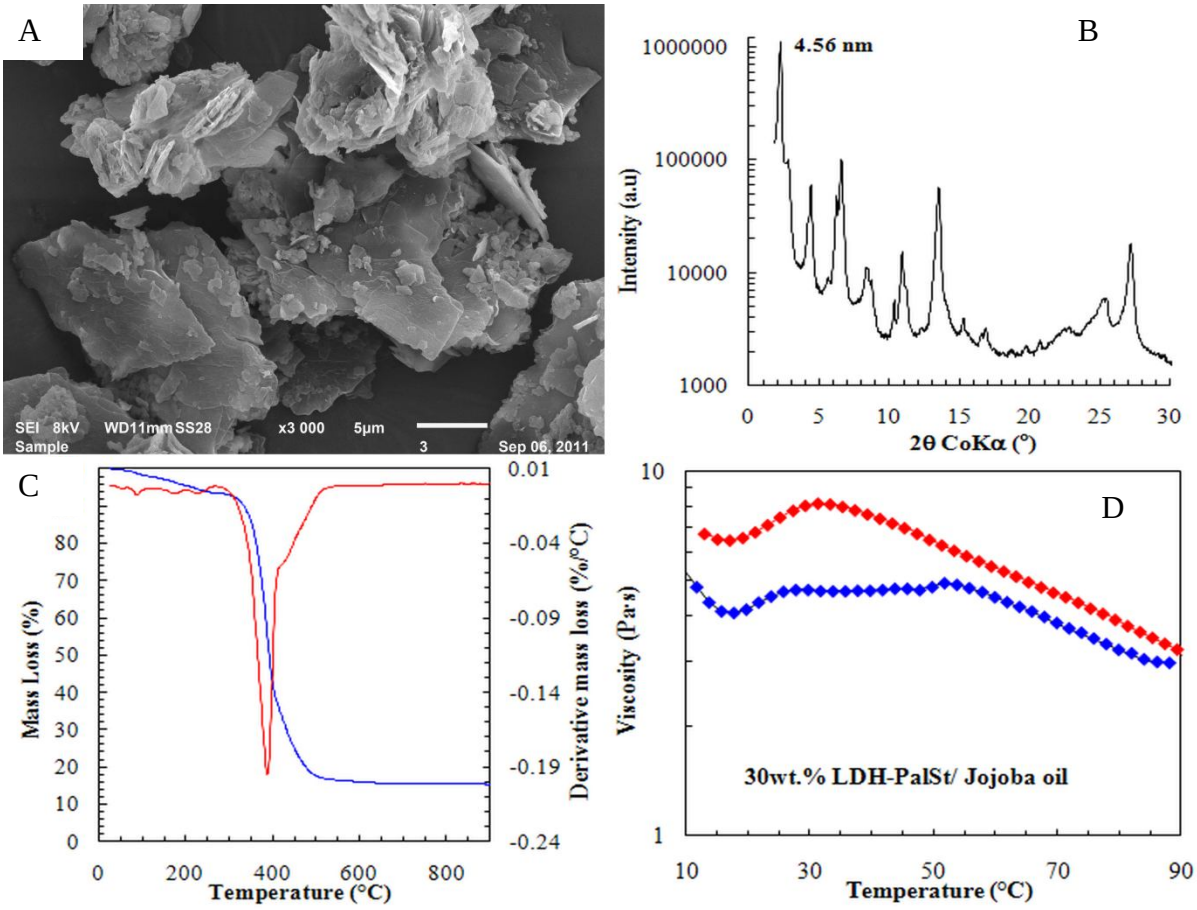

Figure D-12. Summary of subhedral-shaped LDH-Pal-St**:** A – SEM image of morphology of particles**;** B – XRD diffractograms with a d-spacing of 4.56 nm**;** C – TGA data indicating organic content**;** D – **v**iscosity curve as a function of temperature of the derivative 30 wt.% formulation

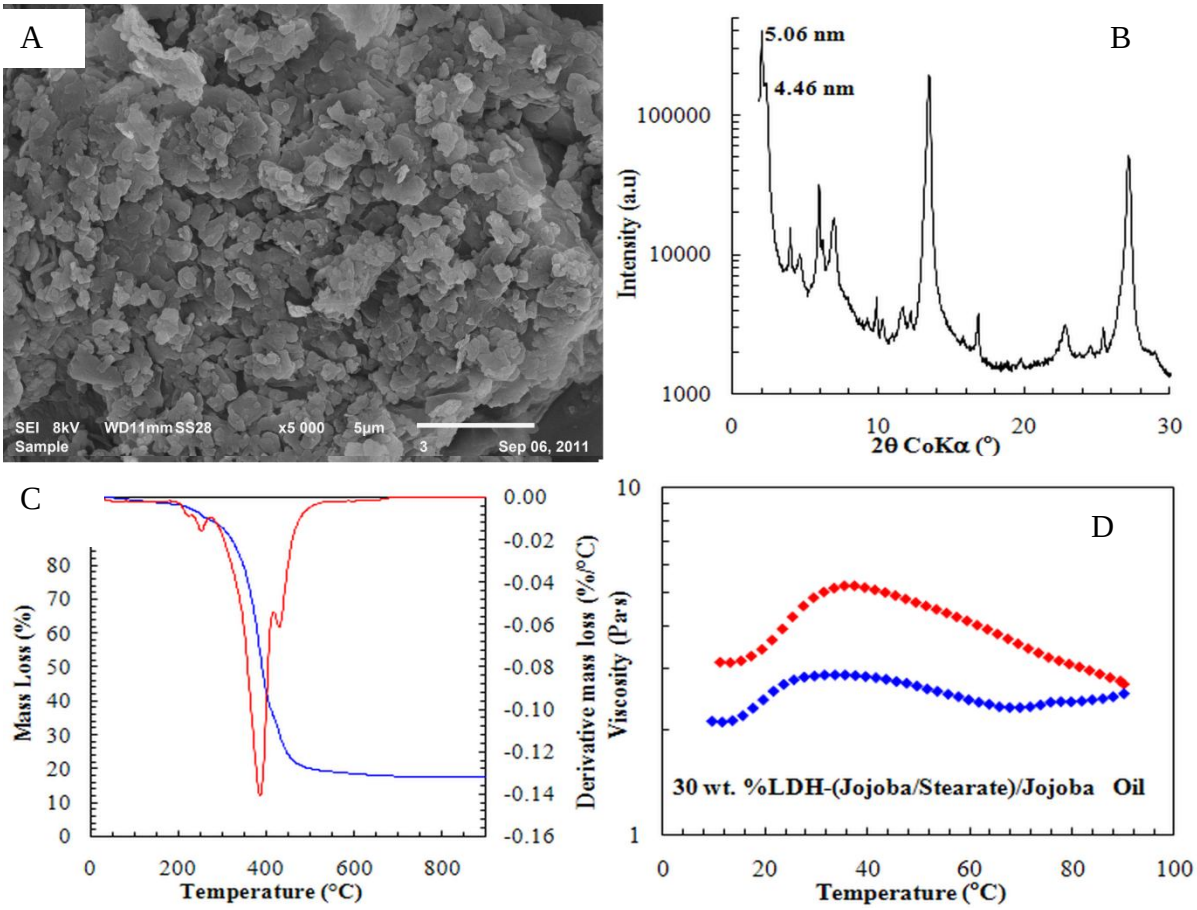

Figure D-13. Summary of subhedral-shaped LDH-(Jojoba/stearate)**:** A – SEM image of morphology of particles**;** B **–** XRD diffractograms with d-spacing**s** of 5.06 and 4.46 nm**;** C **–** TGA data indicating organic content**;** D **– v**iscosity curve as a function of temperature of the derivative 30 wt.% formulation